Tectonophysics 483 (2010) 344–364

Contents lists available at ScienceDirect

Tectonophysics

journal homepage: www.elsevier.com/locate/tecto

Slip partitioning in the northeast Pamir–Tian Shan convergence zone

Bihong Fu [a,*], Yoshiki Ninomiya [b], Jianming Guo [a]

[a] Key Laboratory of the Earth's Deep Interior, Institute of Geology and Geophysics, Chinese Academy of Sciences, Beijing 100029, China
[b] Geological Survey of Japan, National Institute of Advanced Industrial Science and Technology, Tsukuba 305-8567, Japan

ARTICLE INFO

Article history:
Received 16 January 2009
Received in revised form 22 October 2009
Accepted 3 November 2009
Available online 6 November 2009

Keywords:
Late Cenozoic
Slip partitioning
Intracontinental mountain building
Pamir–Tian Shan convergence zone
India–Eurasia collision

ABSTRACT

Based on a detailed analysis of satellite imagery combined with field geologic and geomorphic observations, we have mapped late Cenozoic folds and faults in the northeastern Pamir–Tian Shan convergence zone. It is a unique example to understand intracontinental ongoing mountain building within India–Eurasia collision system. In the front of northeastern Pamir, our investigations reveal that the NW-WNW-trending folds display a right-stepping en echelon pattern and NW-WNW-striking faults are mainly characterized by south-dipping thrusts with an extensive dextral strike-slip component. Drainage systems across the active faults show a systematic right-lateral offset. In contrast, structural style of the ENE trending fold-and-thrust belts are predominated by south–north directed shortening southwest of the Tian Shan. Our results also infer that oblique thrusting accommodates as long-term dextral slip rate of ca. 4.0 mm/yr during the late Cenozoic time north of the Pamir topographic front. Tectono-stratigraphic evidence suggests that the tectonic deformation was initiated at ca. 3–5 Ma in the study area. We suggest that intracontinental mountain building in the Pamir–Tian Shan convergence zone should be attributed to the crustal shortening caused by folding and thrusting as well as block rotation related to strike-slip faulting within the India–Eurasia collision system.

1. Introduction

The northeastern Pamir–Tian Shan convergence zone, consisting of the northeastern Pamir to the south, southwest Tarim basin in the middle, and the Tian Shan to the north, is located in the northwest most part of the India–Eurasia collision zone (see index map in Fig. 1a). The area is characterized by a large topographic relief, whose highest elevation reaches 7710 m (the Kongur Peak in Fig. 1a) in the northeastern Pamir, and elevations abruptly decreasing to 1500–2300 m in the southwest Tarim basin. To the north, elevations increase gradually to ~4000 m in southwest Tian Shan (Fig. 1b). This striking topography has been attributed to the India–Eurasia collision that began ~55 Ma (e.g., Molnar and Tapponnier, 1975; Burtman and Molnar, 1993). Post-collisional convergence took place by southward continental subduction of the Tarim lithosphere beneath the Pamir. The northern Pamir has been thrust north at least 300 km with respect to the rest of Eurasia (Burtman and Molnar, 1993). Geologic and seismic evidence indicates that there is a southward dipping seismic zone beneath the Pamir (Burtman and Molnar, 1993; Fang et al., 1994). Present-day GPS measurements show that the Tian Shan moves 7±2 mm/yr southward with respect to the interior of Tarim in the Kashi region (Shen et al., 2000). One giant earthquake (1902 Ms=8.3 Atushi earthquake as shown in Fig. 1a) and 30 moderately strong earthquakes (8>Ms>6) occurred along this convergence zone in recent 100 years (Feng, 1997; Tian et al., 2006). Therefore, it is a critical region to understand the ongoing intracontinental mountain building and unique structural deformation resulting from the India–Eurasia collision. However, the regional kinematics of the late Cenozoic deformation is poorly understood in the northeastern Pamir–Tian Shan convergence zone because of its remoteness and inaccessibility.

In this study, we document the late Cenozoic deformations based on the interpretation and analysis of satellite remote sensing data combined with the field geologic and geomorphic observations in the northeastern Pamir–Tian Shan convergence zone. We also discuss the timing and kinematics of the late Cenozoic deformations.

2. Geological setting

The northern boundary of the Pamir is marked by the northern Pamir thrust zone (NPT in Fig. 1a), a south-dipping arcuate thrust zone, which consists of a series of thrust faults. It represents the present boundary between the Pamir and southwest Tarim basin (Fig. 1a). North of the topographic front northeastern Pamir, several rows of folds and faults trending NW in a right-stepping en echelon pattern. To the north, three rows of elongate Cenozoic folds and faults north of Kashi display a left-stepping en echelon pattern (Fig. 1a). ENE trending fault zones display north-dipping thrusts and south-dipping back thrusts in the southwestern margin of the Tian Shan (Fig. 1a).

* Corresponding author. Division of Tibetan Plateau Research, Key Laboratory of the Earth's Deep Interior, CAS, Institute of Geology and Geophysics, Chinese Academy of Sciences, P.O. Box 9825, Beijing 100029, China. Tel.: +86 10 8299 8339; fax: +86 10 8299 8229.
E-mail address: fubihong@mail.iggcas.ac.cn (B. Fu).

0040-1951/$ – see front matter © 2009 Elsevier B.V. All rights reserved.
doi:10.1016/j.tecto.2009.11.003

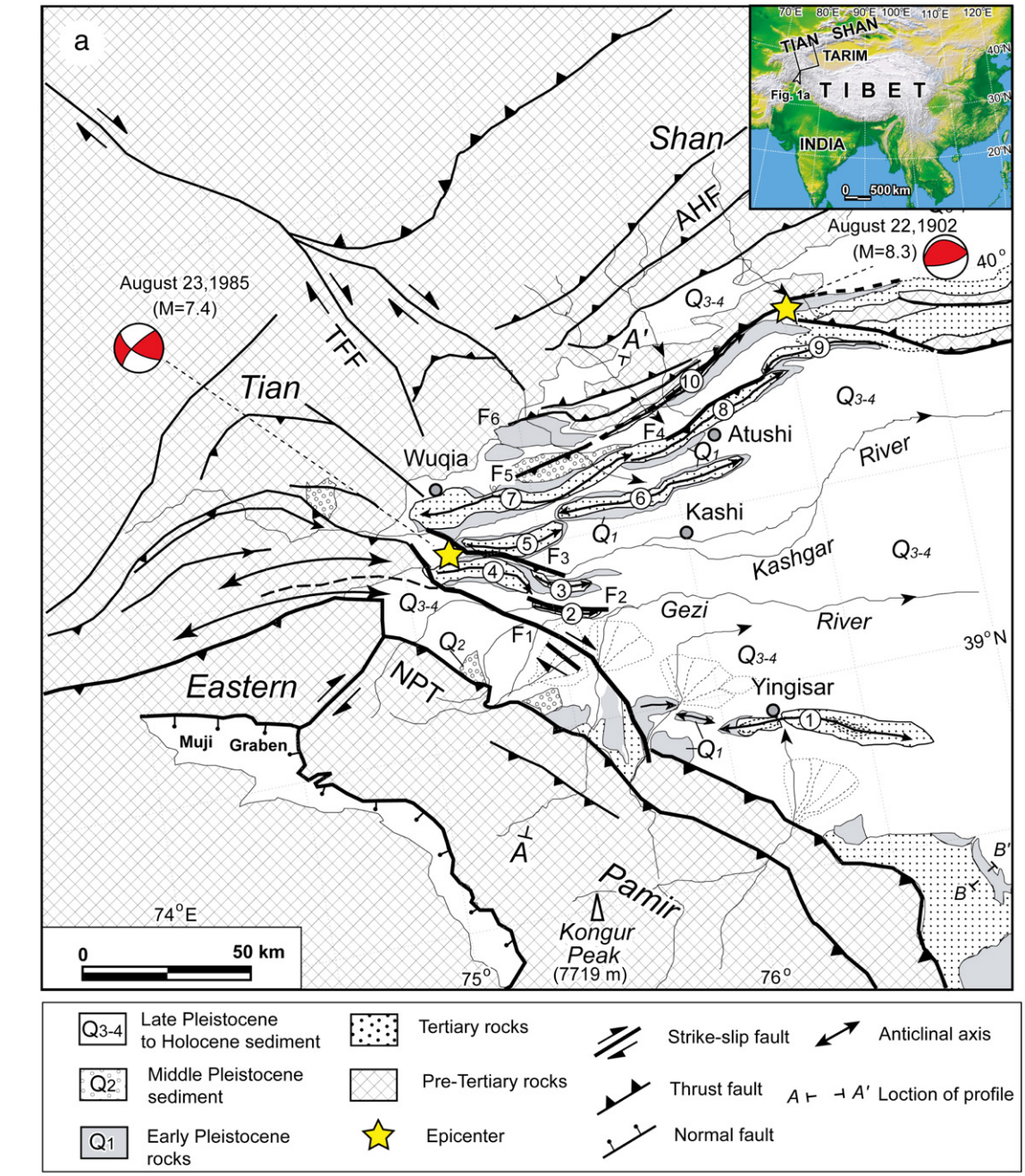

Fig. 1. (a) A Cenozoic tectonic map of the northeastern Pamir–Tian Shan convergence zone constructed from an analysis of satellite images and field observations. NPT: north Pamir thrust; AHF: Aheqi fault; TFF: Talas-Fergana fault; ①Yingisar anticline; ② Ubulake anticline; ③ Tumuan anticline; ④ Mushi anticline; ⑤ Mingyaole anticline; ⑥ Kashi anticline; ⑦ Kerato anticline; ⑧ Atushi anticline; ⑨Bapanshuimo anticline; ⑩ Tashipishake anticline. (b) A geologic cross-section showing the structural styles of the fault-and-fold belt in the northeastern Pamir–Tian Shan convergence zone (subsurface structural style interpreted from the unpublished seismic profile provided by the Xinjiang Bureau of Petroleum, CNPC). For location see section A–A′ in Fig. 1a.

The Aheqi fault zone (AHF in Fig. 1a) forms the boundary between the Tian Shan and Tarim basin (Jia et al., 1998). In the northwestern part of the study area, the NNW striking Talas-Fergana fault zone forms the boundary between the western and central Tian Shan (Fig. 1a). Burtman et al. (1996) estimated a late Cenozoic slip rate of 10 mm/yr along this right-lateral strike-slip fault zone. Present-day GPS data indicated a shortening rate of about 18–20 mm/yr across the western Tian Shan (Abdrakhmatov et al., 1996; Shen et al., 2000).

Up to 10 km Cenozoic strata accumulated in this convergence zone and form the deepest Cenozoic depression in the Tarim basin (Fig. 1b, Wang et al., 1992). Lower Tertiary (here designed E) strata up to 800 m consist of greyish green and brownish red sandstone, siltstone and argillite, interbedded with marine limestone and gypsum. *Branchicontes jermenjewi*, *Cardium* sp., *Fergania ferganensis*, *Corbula asiatica*, and *Ostrea* (*Turkostrea*) *strictiplicata* have been found from the strata (XJUARRSCG, 1981). Continental Miocene (N_1) strata are characterized by brownish red and greyish green sandstone, siltstone, argillite with gypsum and are up to 6050 m thick (Fig. 2). These sedimentary rocks contain fossils, such as *Cyprideis littoralis*, *Darwinula stevensoni* and *Limnocythere iliensis* (XJUARRSCG, 1981). Pliocene (N_2) strata are mainly composed of yellowish brown and light yellow argillite, siltstone, sandstone and conglomerate with a thickness ranging from 500 to 3400 m (Figs. 2 and 3a; BGMXJ, 1993). Many fossils, such as *Ilyocypris errabundis*, *Candona* (*Candona*) *neglecta*, *Candona* (*Pseudocandona*) *subequalis* and *Eucypris notabilis* etc., have been found (XJUARRSCG, 1981).

Quaternary deposits are widely developed in the front of the Pamir and Tian Shan (Fig. 2). Quaternary sequences can be divided into four groups or formations. They are lower Pleistocene (Q_1, 2.6 Ma to 1.1 Ma), middle Pleistocene (Q_2, 1.1 Ma to 0.12 Ma), upper Pleistocene (Q_3, 0.12 Ma to 12 ka) and Holocene (Q_4, 12 ka to present) based on detailed lithostratigraphy, existing biostratigraphic (XJUARRSCG, 1981; BGMRXJ, 1993) and magneostratigraphic data (Chen et al., 1994; Chen et al., 2002; Sun et al., 2004; Scharer et al., 2006), and

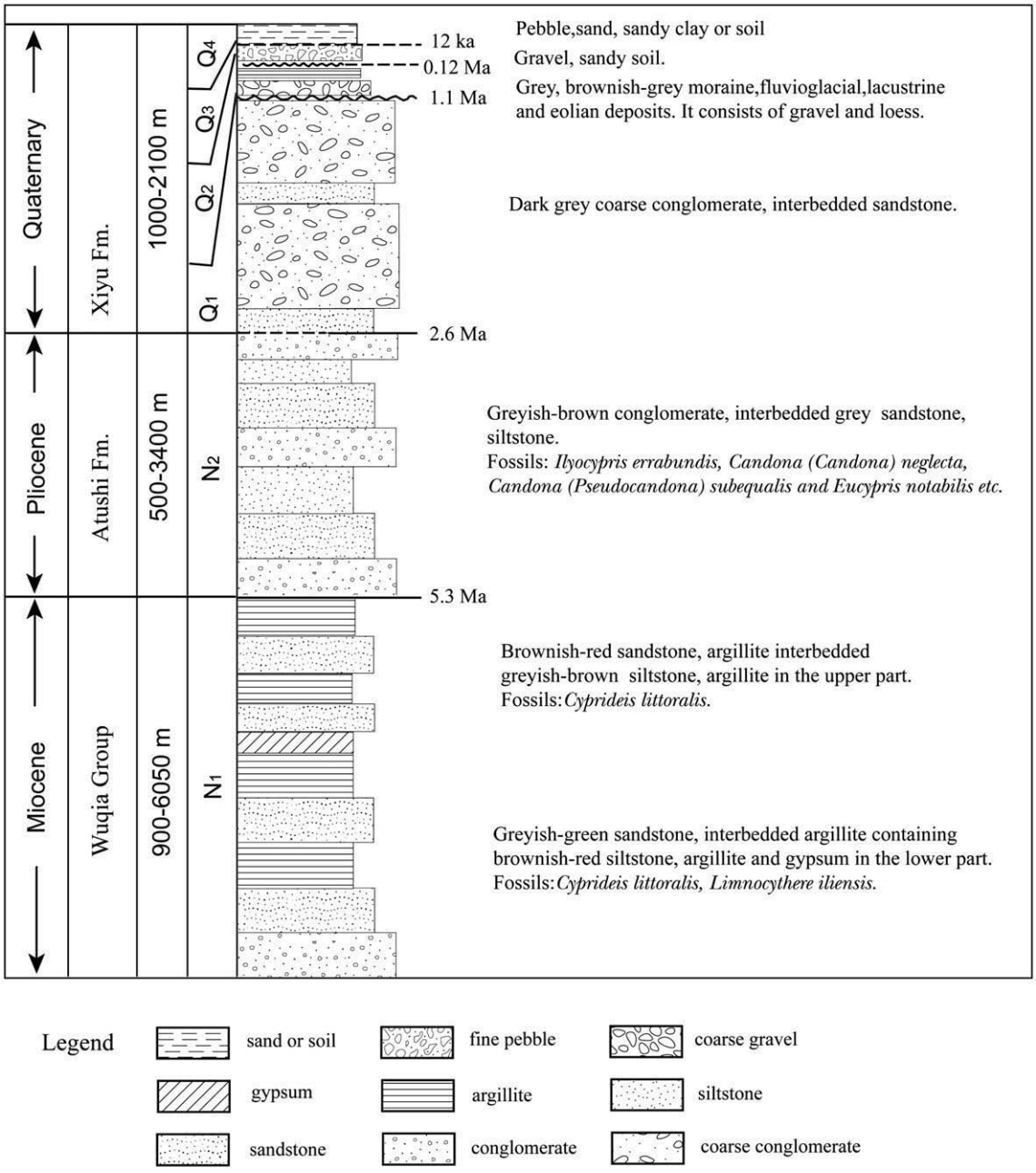

Fig. 2. Neogene stratigraphy exposed in the study region from Miocene to Quaternary. This was according to Sobel (1999) and XJUARRSCG (1981).

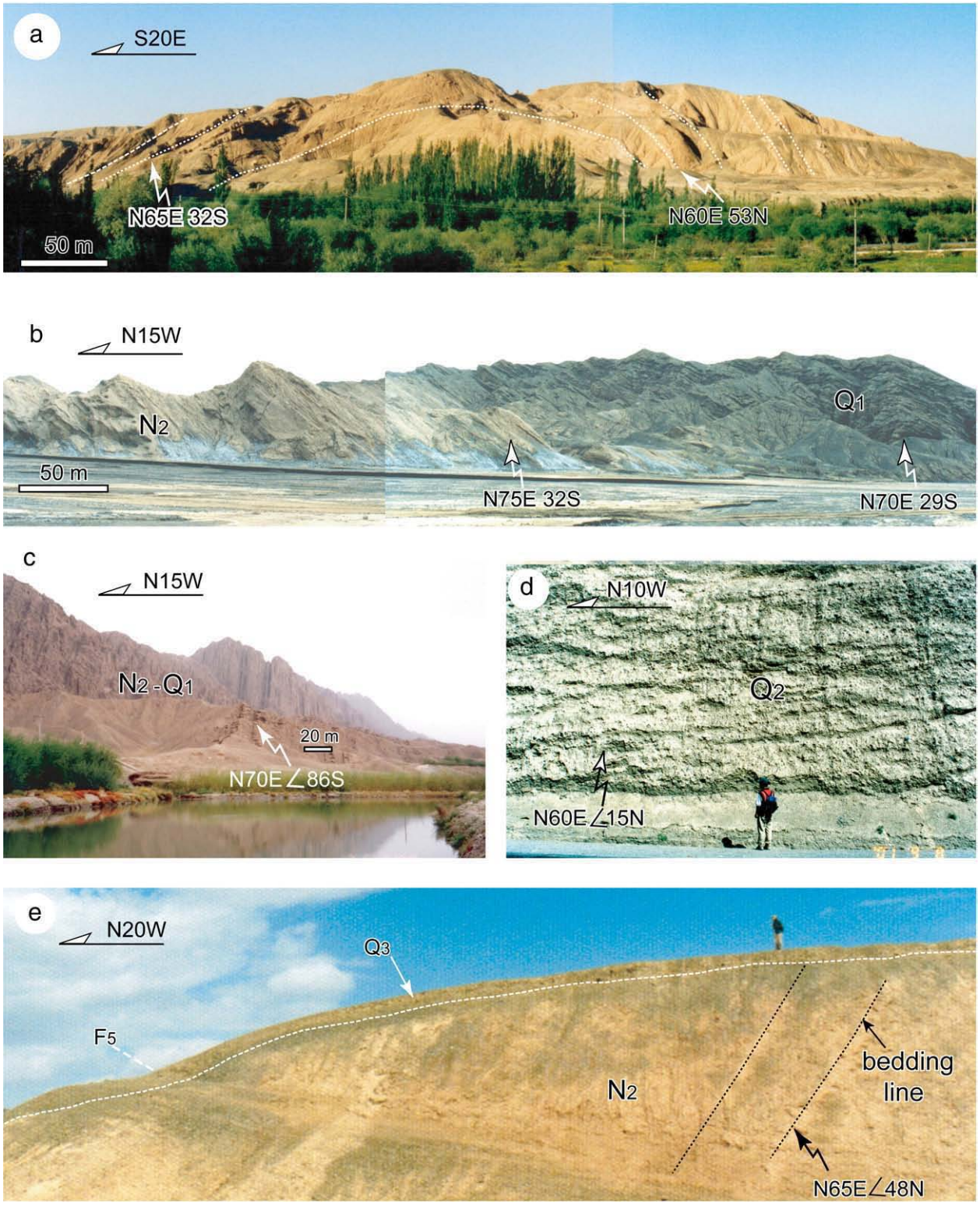

Fig. 3. Photographs showing the late Cenozoic deposits in the northeastern Pamir–Tian Shan convergence: (a) Miocene sequences observed at the core of the Atushi anticline (for location see Loc.9 in Fig. 12b). (b) Conformable contact between Pliocene (N_2) sandstones and lower Pleistocene (Q_1) conglomerate observed at the south limb of Tuogerming anticline (for location see Loc. 11 in Fig. 12b). (c) Steep-dipping lower Pleistocene (Q_1) conglomerate observed at the southern limbs of the Tashipishake anticline (For location see Loc. 10 in Fig. 12b). (d) Middle Pleistocene (Q_2) deposits observed at the northern limbs of the Kashi anticline (for location see Loc. 5 in Fig. 11b). (e) Gentle folding of upper Pleistocene deposits (Q_3) occurred in the northern limbs of the Atushi anticline (for location see Loc. 7 in Fig. 12b).

radiocarbon, cosmic ray exposure and TL dating (Feng, 1997; Brown et al., 1998; Fu et al., 2003), as well as our field observations (Lin et al., 2002; Fu et al., 2003). The contacts between Q_1 and Q_2, Q_2 and Q_3, Q_3 and Q_4 are usually marked by unconformities (XJUARRSCG, 1981; Chen et al., 1994). Lower Pleistocene (Q_1) deposits are mainly dark grey gravel to boulder conglomerates 1000 to 1795 m thick (Fig. 3b and c). These coarse and thick conglomerates are interpreted as a molasse deposited in the front of the Pamir and the Tian Shan. There is a regional unconformity between early Pleistocene (Q_1) and middle Pleistocene (Q_2) strata as shown in Fig. 3. Growth strata are also

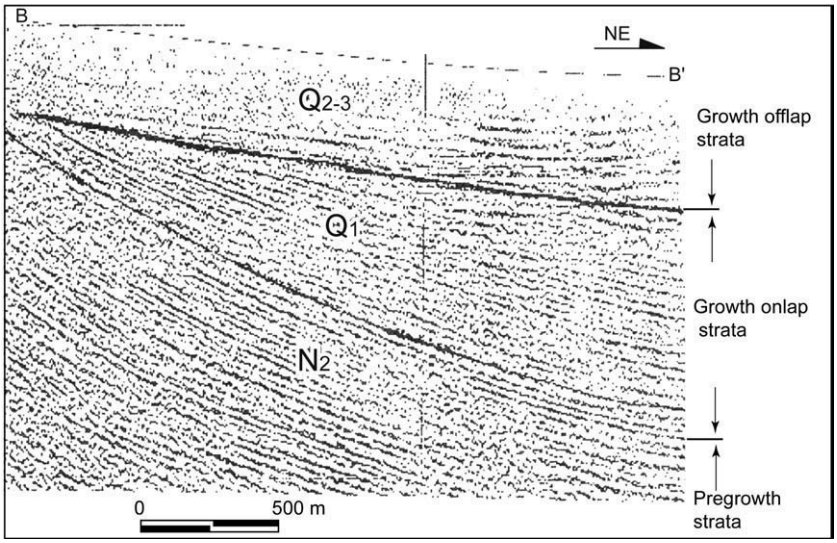

Fig. 4. Seismic reflection profile displays the growth strata in the upper Pliocene (N_2) and lower Pleistocene (Q_1) sequences (after Dong and Xiao, 1998). For location see B–B′ in Fig. 1a.

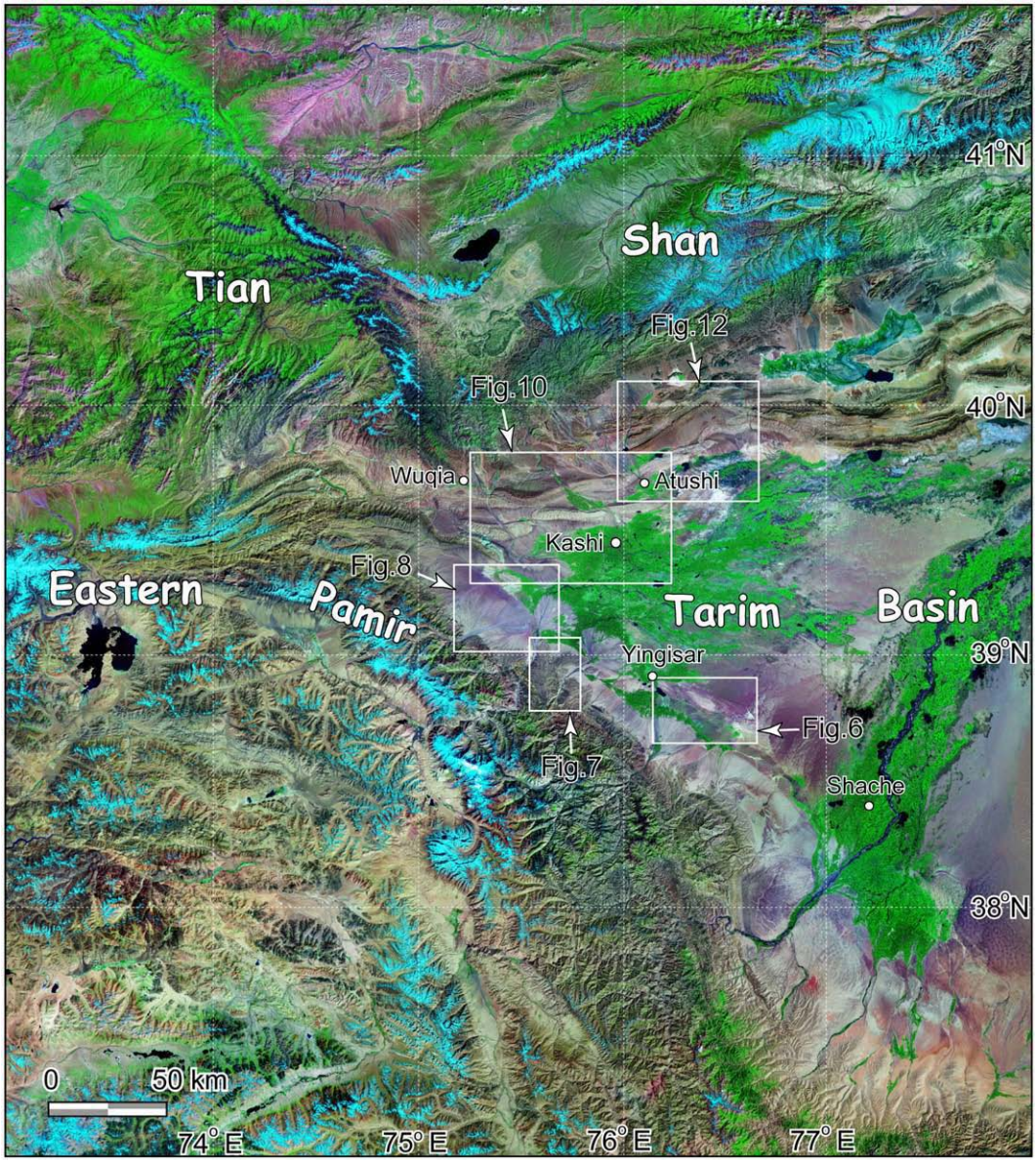

Fig. 5. A Landsat ETM/TM mosaic image showing the structural features in the northeastern Pamir–Tian Shan convergence zone.

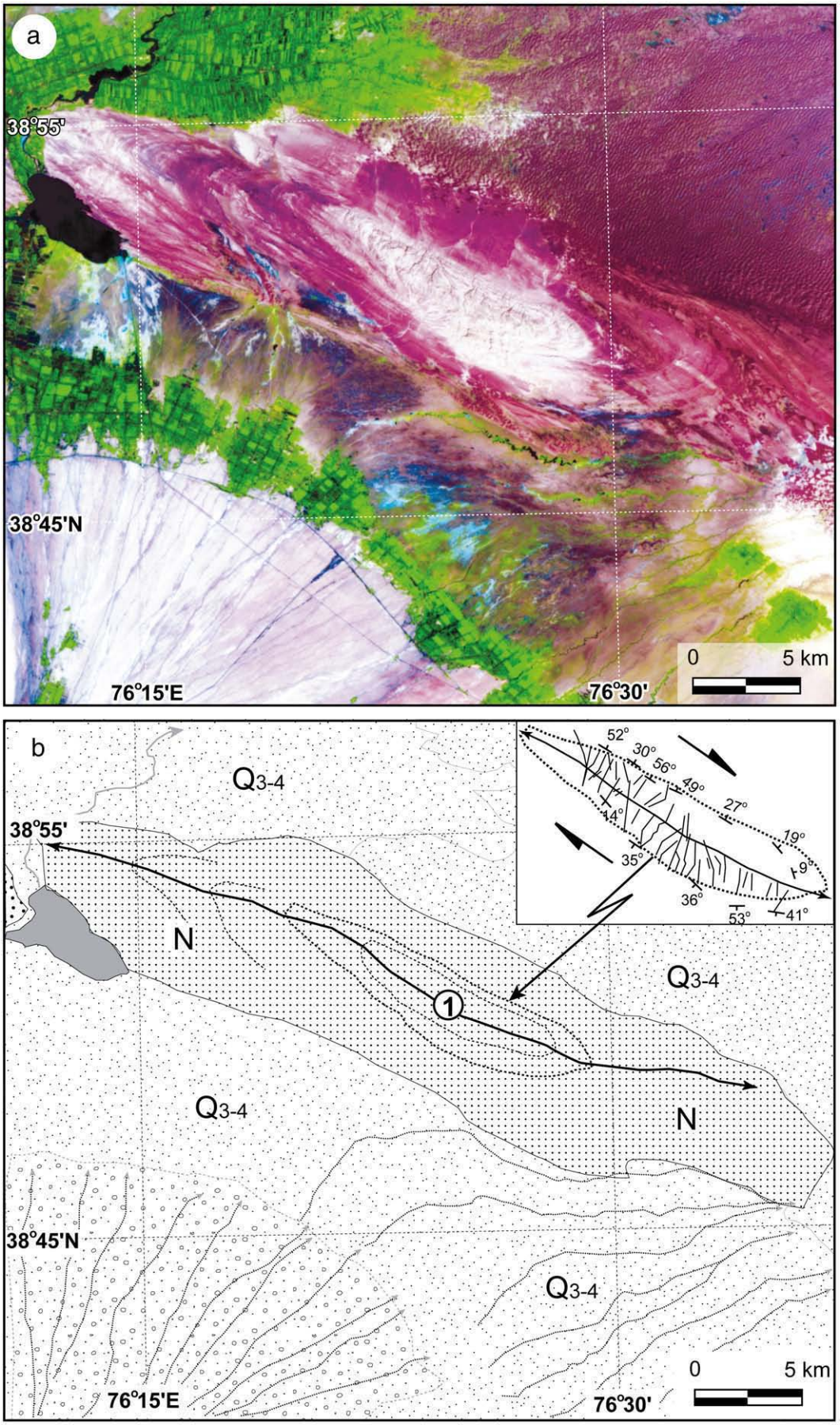

Fig. 6. A Landsat ETM image (a) and a geologic interpretative map (b) showing the deformation features along the Yingisar anticline. Note that the extensional fractures are perpendicular to the anticlinal axis along this anticline. For location see Fig. 5.

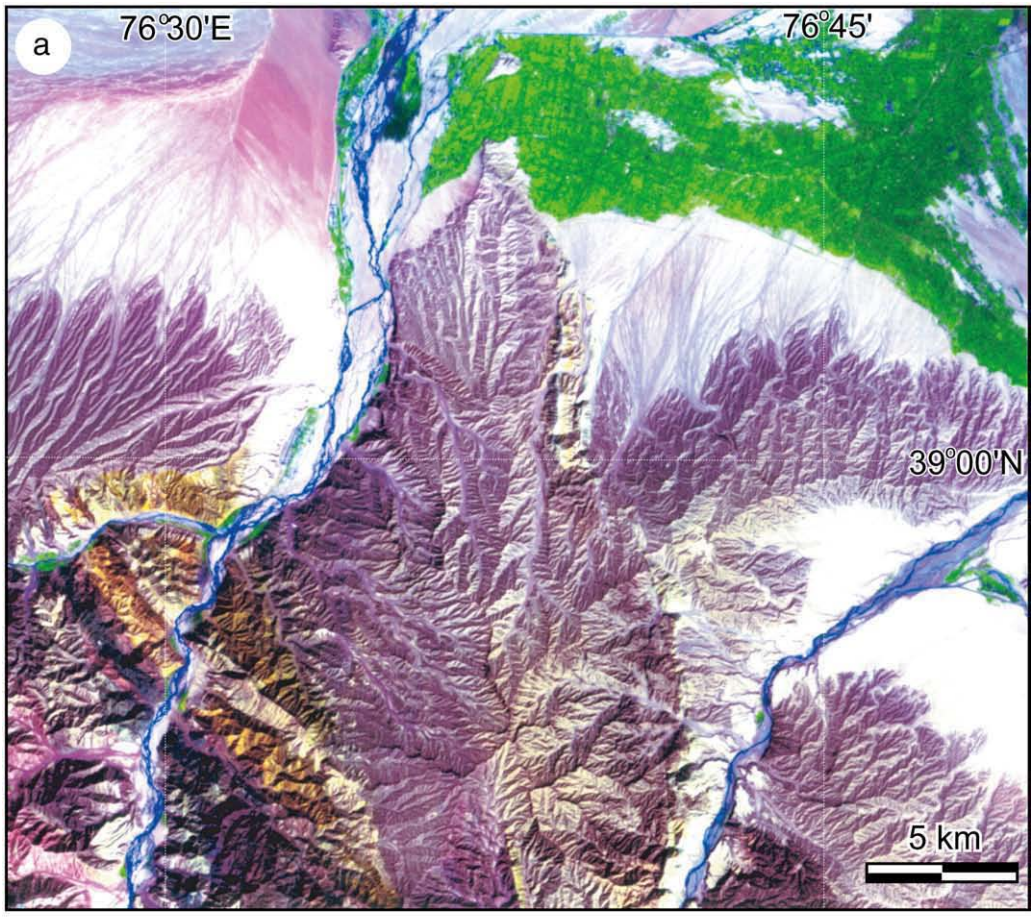
a
76°30'E
76°45'
39°00'N
5 km

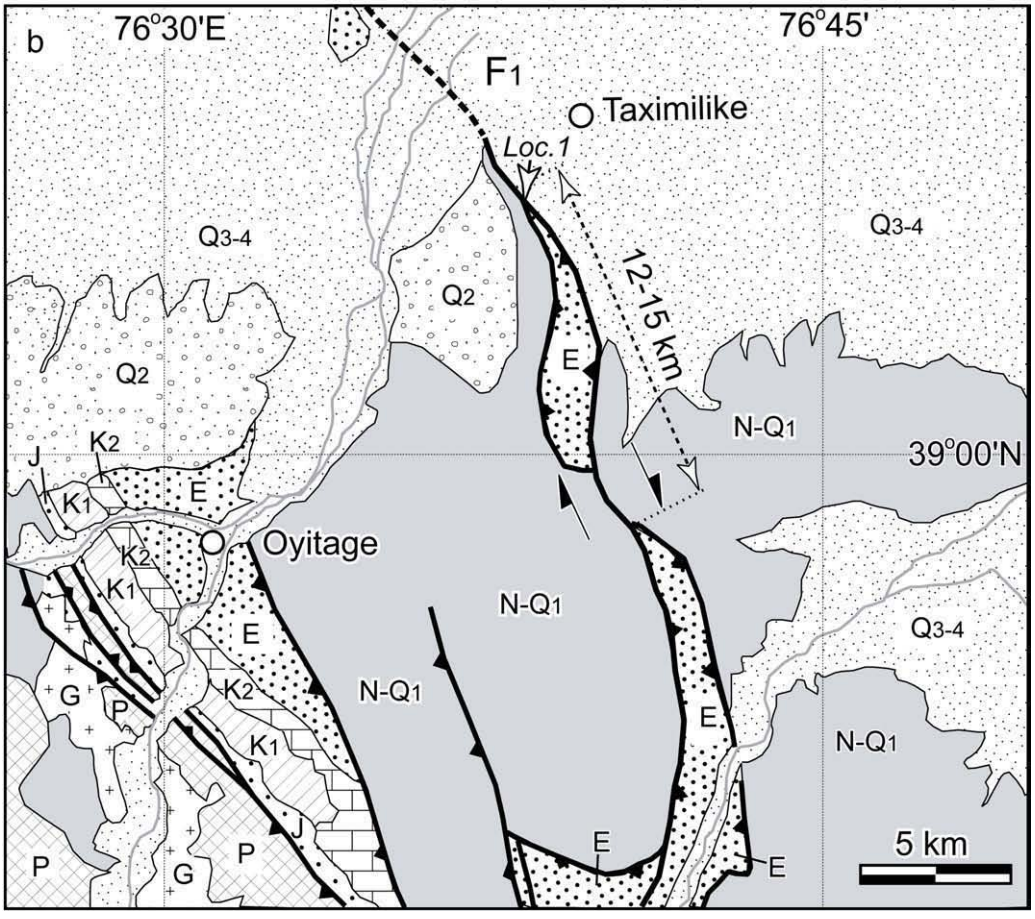
b
76°30'E
76°45'
F1
Taximilike
Loc.1
12-15 km
Oyitage
39°00'N
Q3-4
Q2
E
N-Q1
K2
K1
J
G
P
5 km

widely developed in the upper part of Pliocene to the lower part of Lower Pleistocene conglomerate in the front of the Pamir as shown on a seismic reflection profile (Fig. 4). Middle Pleistocene (Q_2) deposits consist of the moraine, fluvioglacial, lacustrine and alluvial–fluvial deposits that are 10 to 30 m thick (Figs. 2 and 3d). They are usually semi-consolidated or unconsolidated, and occur about 40 to 200 m above the modern streambeds. Upper Pleistocene (Q_3) deposits are composed of early and late tillte, fluvioglacial deposits and alluvial deposits, which are usually unconsolidated (Figs. 2 and 3e). They are 30–100 m thick, and occur about 6 to 15 m from the modern streambeds. Holocene (Q_4) strata usually includes unconsolidated alluvial, Aeolian, and talus deposits 1 to 20 m thick (BGMXJ, 1993).

3. Methods

Landsat Enhanced Thematic Mapper/Thematic Mapper (ETM/TM) data (15–30 m spatial resolution) (Fig. 5), and Advanced Spaceborne Thermal Emission and Reflection Radiometer (ASTER) Visible and Near Infrared (VNIR) data (15 m spatial resolution) were processed using the ER-Mapper image processing software. Stereoscopic pairs from single scene Landsat ETM/TM also were created using the method described by Fu et al. (2004).

In this study, Landsat ETM/TM and ASTER images at a variety of scales ranging from 1:50,000 to 1:250,000 were used to interpret the Cenozoic folds and faults before conducting field survey (Figs. 5, 6a, 7, 8, 9a, 10a, 11a, and 12a). Interpretations of these images were verified and farther investigated in the field (Figs. 3, 9b, 13, 14 and 15). Furthermore, some published seismic reflection profiles were re-interpreted to understand geometry of fold-and-fault belts (Figs. 4 and 16).

4. Late Cenozoic folds and faults

Late Cenozoic deformational features are described from south to north and east to west in the following sections.

4.1. Folds

Three rows of NW-WNW-trending Cenozoic folds occurred in the south part of the Pamir–Tian Shan convergence zone (Fig. 1a). They are Yingisar, Ubulake, Mushi and Tumuan anticlines from southeast to northwest, which display a right-stepping en echelon pattern (①, ②, ③ and ④ respectively in Fig. 1a). Folded lower Tertiary to lower Pleistocene strata occur in these anticlines which have gentle south limbs (15 –40°) and steep north limbs (35–70°). The WNW-trending Yingisar anticline has deformed Q_1 strata (Fig. 1a) and Miocene to Pliocene strata exposed in the core of this anticline (Fig. 6b). Extensional fractures are perpendicular to fold axis. The attitude of both folded limbs appears asymmetric in the central part, which suggests that fold was influenced by complex transpressional strains (Fig. 6b). The Ubulake, Mushi and Tumuan anticlines folded lower Tertiary to Q_1 strata (Fig. 11b).

In contrast, Cenozoic folds north of Kashi are characterized by three rows of the elongate folding zones trending E–W to ENE. These three rows of folding zones display a left-stepping en echelon pattern (Fig. 1a). They are Mingyaole, Kashi, Krato, Atushi, Bapanshuimo and Tashipishake anticlines (⑤, ⑥, ⑦, ⑧, ⑨ and ⑩ respectively in Fig. 1a). These folds have relatively gentle south limbs and steep north limbs except for the Tashipishake anticline (Figs. 1b and 16a). It noteworthy that overlapping part of Atushi anticline and Bapanshuimo anticline displays an S-shaped bend (⑧ and ⑨ in Figs. 1a and 12b), suggesting that they were deformed by S–N compression accompanied by lateral propagation along the southwestern margin of the Tian Shan. Miocene to Q_1 strata are deformed in these folds (Figs. 2, 11b and 12b). Q_2 to Q_3 strata also have been partly deformed in some of these folds (Fig. 3d and e). For example, Q_2 strata are deformed in the north limb of Kashi anticline as observed at Loc.4 (Fig. 3d), and Q_3 alluvial deposits are deformed along the Atushi anticline (Fig. 3e).

4.2. Faults

Many faults occur along the northeastern Pamir–Tian Shan convergence zone (Fig. 1a).

4.2.1. Northeastern front of the Pamir

Four main faults have been identified from satellite images in the front of the northeastern Pamir (Fig. 1a). We call them the Northern Pamir Thrust (NPT), F_1, F_2 and F_3 faults.

NPT shows an arcuate trace which strikes NW in the east to near E–W in the southwest (Fig. 1a). The fault juxtaposes the Paleozoic strata on the Mesozoic–Cenozoic strata (Fig. 1b).

Of particular note is the F_1 fault zone that trends N35°W, and from the satellite images appears as a sharp lineament traversing the Quaternary alluvial fans in the northeastern front of the Pamir (Figs. 1a, 5 and 7a). This fault has displaced lower Tertiary to lower Pleistocene strata near Taximilike where a dextral offset of lower Tertiary (E) and N_2–Q_1 is about 12–15 km (Fig. 6). A field study indicated that it is a right-lateral strike-slip fault with a steep dipping (80° NE) as shown on Figs. 13a and 13b. Northwestward, east facing fault scarps are well developed in the late Quaternary alluvial fan deposits (Figs. 7 and 8). A graben develops along the fault zone (Fig. 8a). The stream channels and gullies across the fault scarps are offset or deflected dextrally along the F_1 fault zone (Fig. 8). Northeast-facing fault scarps measured in the field are from 50 cm to 3.5 m high (Fig. 9c). The ^{14}C dating age of charcoal collected from alluvial fan deposits yielded a date of 891 ± 56 yr BP along the F_1 fault zone (Fig. 13f, ^{14}C dating age measured by Tono Geoscience Center, Japan Nuclear Cycle Development Institute using the AMS method). Generally, an individual upstream channel has 2 to 3 abandoned offset downstream channels that mark the progressive displacement along the fault (Fig. 9b). The offset of small stream channels and gullies along the southeastern part of the fault vary from 4 to 20.4 m (Fig. 9b). They can be divided into four groups: small gullies showing offsets of 4.0 to 4.9 m, moderate stream channels or gullies with offsets of 5.4 to 6.8 m, large ones with and 8.9 to 12.8 m, and largest ones with offsets of 14.3 to 20.4 m. The most obvious offsets of drainages along the F_1 fault zone appear in its northwest part where several large stream channels are displaced dextrally (Fig. 10a). The dextral offsets of stream channels a–a′, b–b′ and c–c′ are 8000, 3430 and 1700 m respectively (Fig. 10b). The 10–15 m high fault scarps occur along the fault zone (Fig. 13d). They show the cumulative displacement along the main fault zone, where the longer the length and bigger the width of stream channel, the larger the offset. This is interpreted as being the older the stream channel, the larger the offset. Similar results were found along the active strike-slip faults in the intermontane basin in the eastern Tian Shan (Lin et al., 2002).

F_2 and F_3 faults trend N40–60°W in the northern limbs of the Ubulake and Tumuan–Mushi anticlines, respectively (Figs. 1a and 11). They appear as clear lineaments on the satellite images (Figs. 10a and 11a). These south-dipping thrusts cut upright or overturned strata on northern limbs of folds (Fig. 1b). A field study shows that the F_2 fault is active and has displaced late Quaternary alluvial deposits. The fault scarp is about 50–75 cm high, and lateral offset of gullies that cross the faults are about 1.0–1.5 m. These displacements were probably caused by the latest earthquake event. The 1985 Ms 7.4 Wuqia earthquake occurred along the F_3 fault zone (epicenter showing in Fig. 1a, Feng, 1997). It developed

Fig. 7. Landsat ETM imagery (a) and geologic interpretative map (b) showing the offset of lithologic sequences along the southeast part of the F_1 fault zones. Note that the right-lateral offset of Tertiary sequence is about 12 to 15 km. For location see Fig. 5.

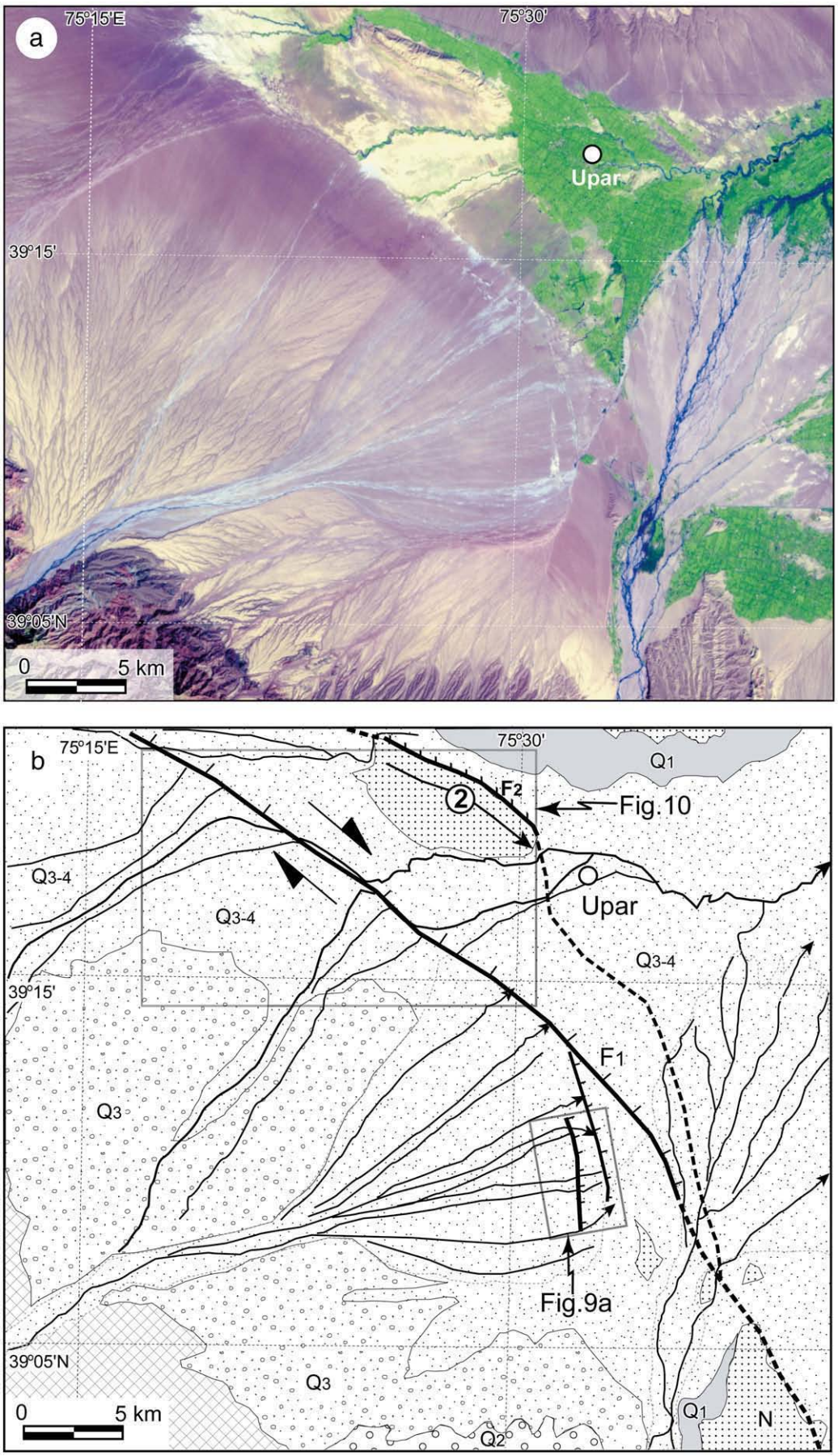

Fig. 8. Landsat ETM imagery (a) and geologic interpretative map (b) display the geomorphologic features of the F_1 and F_2 fault zones. For location see Fig. 5.

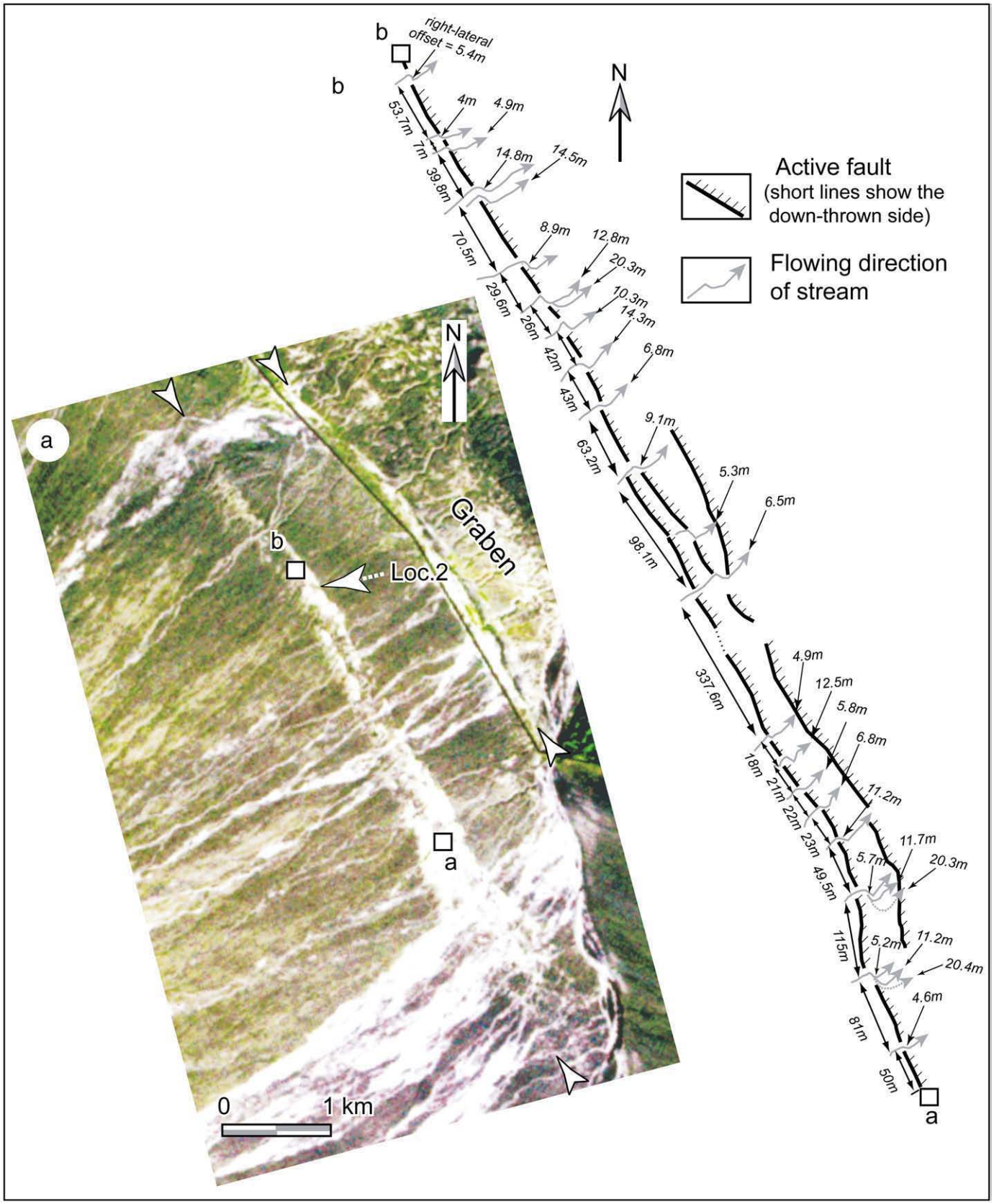

Fig. 9. (a) ASTER imagery shows the geomorphologic features of southeast segment of the F_1 fault. The fault scarps indicated by arrows. Note that a graben appears in the upper right of the image. (b) Fault scarps and the systematic right-lateral offset of gullies along the F_1 fault zone measured in the field. This is the location indicated by squares on Fig. 9a.

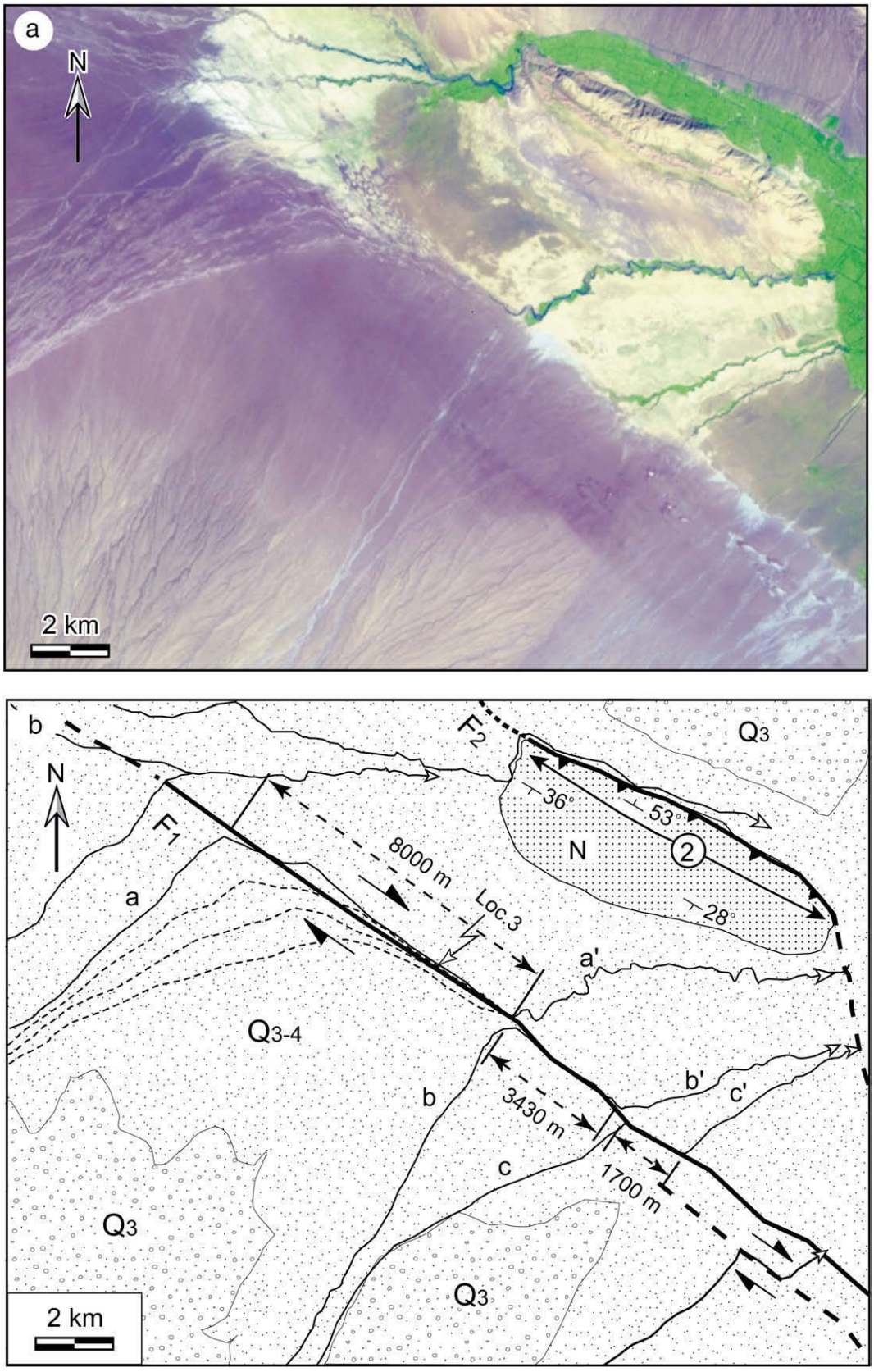

Fig. 10. A Landsat ETM image (a) and an interpretative map (b) showing the offset of streams along the northwest segment of the F_1 fault zone and geomorphic features of F_2 fault. Note that the main streams a–a′, b–b′, c–c′ have been dextrally offset, and the amounts of displacement are 8000 m, 3430 m and 1700 m along the F_1 fault respectively. The F_2 fault displaced the northern limb of the Ubulake anticline. For location see Fig. 8b.

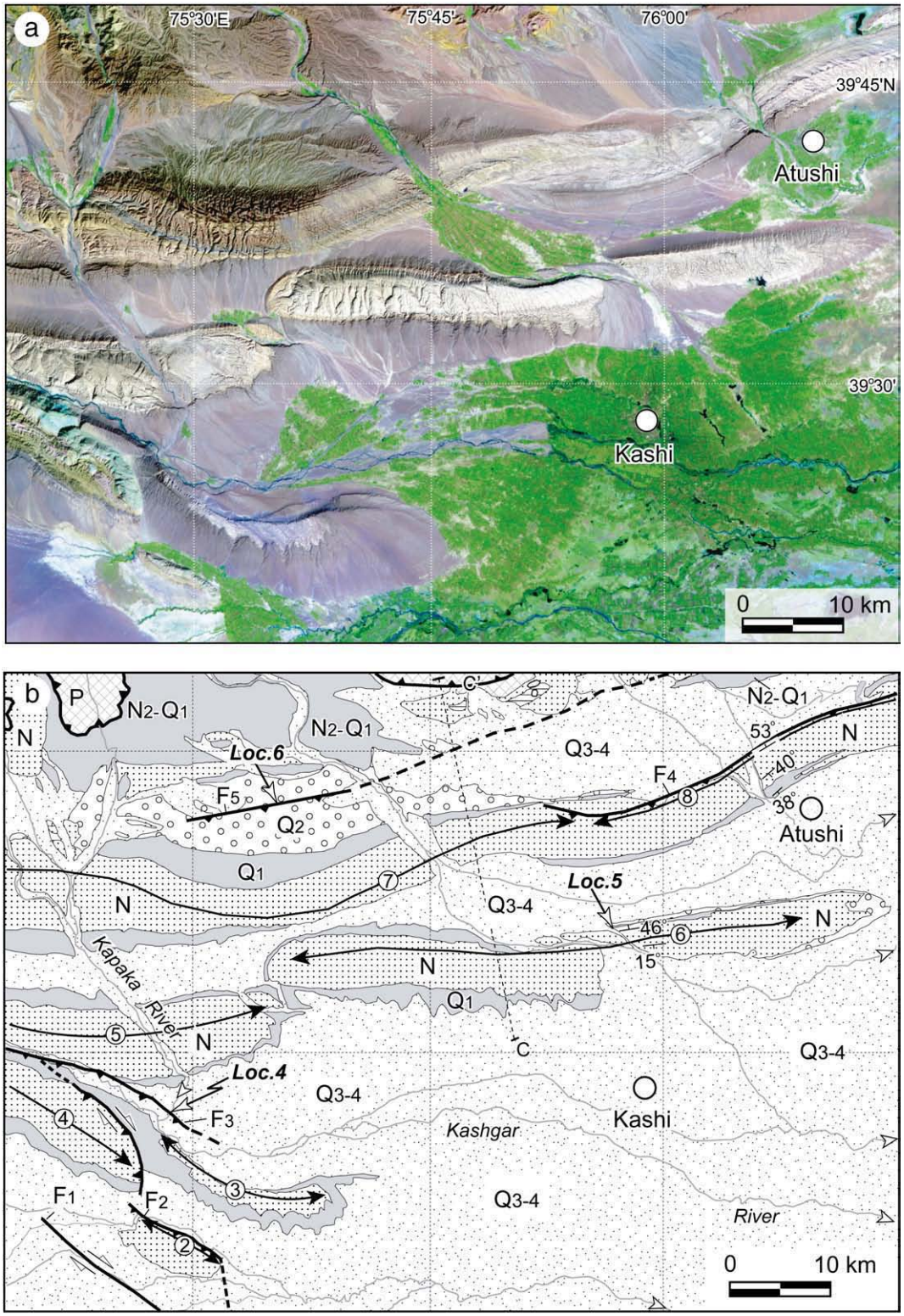

Fig. 11. A Landsat TM image (a) and a geologic interpretative map (b) showing the folds and faults to north of the Kashi. Location is shown in Fig. 5. See text for details.

along the north limbs of the Tumuan and Mushi anticlines and displaced Tertiary to Holocene deposits (Fig. 11). For example, three active faults displaced a late Quaternary terrace along the F_3 fault zone as we observed at eastern bank of the Kapaka River (Figs. 14a, b and c). The Fa fault displaced the youngest sequence of late Quaternary terrace deposits and formed a 1.5 m high fault scarp (Figs. 14a and c), which represents co-seismic displacement related to the 1985 Wuqia earthquake (Fig. 1b; Feng et al., 1987). But the Fb and Fc faults did not displace the youngest terrace deposits (Fig. 14c), and are likely associated with older seismic events.

4.2.2. Southwestern margin of the Tian Shan

There are series of ENE-striking faults along the southwest margin of the Tian Shan (F_4, F_5, F_6 and AHF in Fig. 1a).

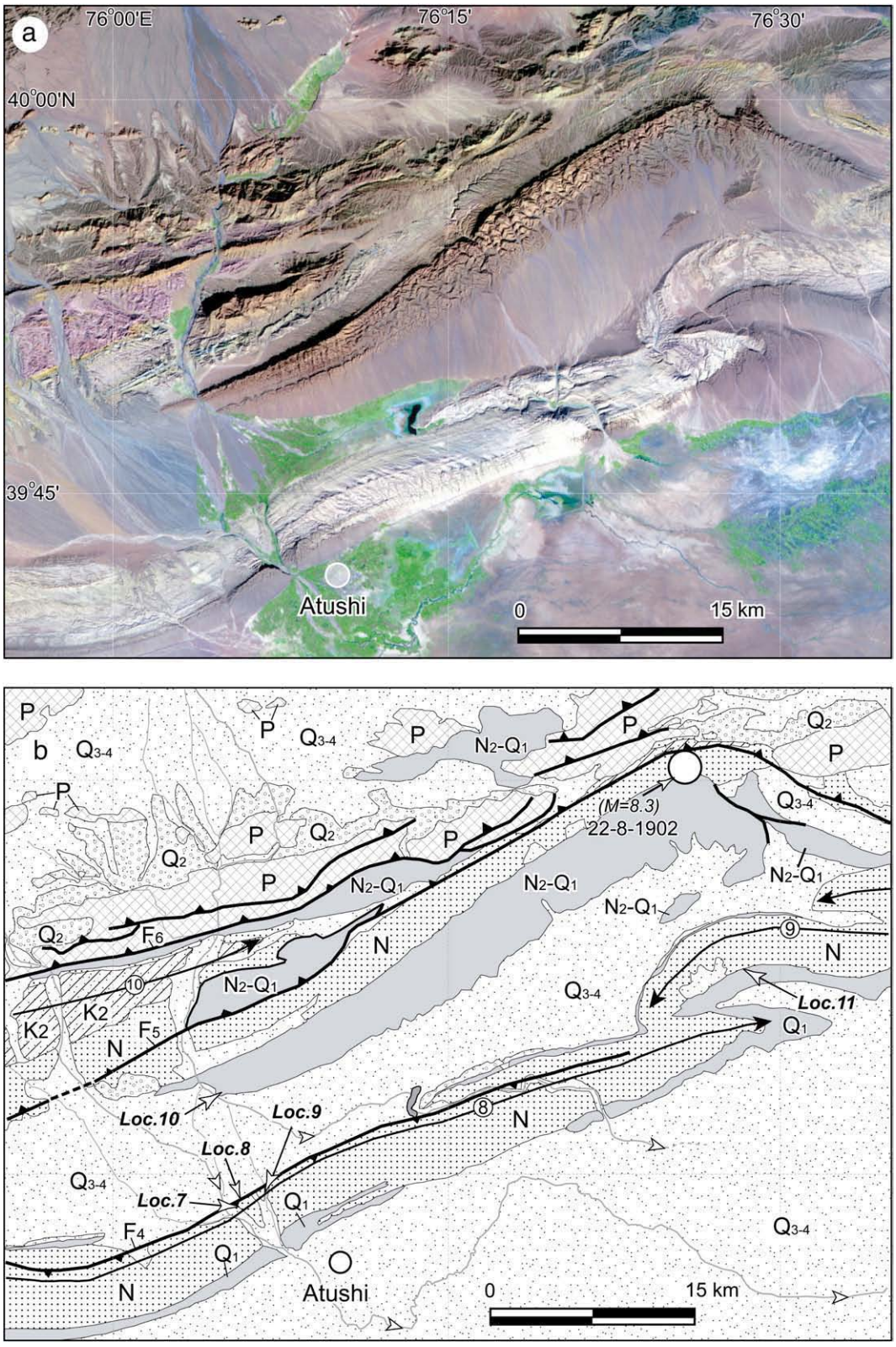

Fig. 12. A Landsat TM image (a) and a geologic interpretative map (b) showing the late Cenozoic folds and faults in the southwest margin of the Tian Shan. For location see Fig. 5.

Fig. 13. Photographs showing the occurrence of F_1 fault zone. (a) Fault plane of F_1 strikes N40°W and dips 80°NE at Loc.1. For location see Fig. 7b. (b) Close view of fault plane. Slickenside line is indicated by a white arrow. (c) Fault scarp with 3 m high and right-lateral offset of gully along the active fault observed at Loc.2. The arrow indicates the flowing direction. For location see Fig. 9a. (d) Fault scarp with 15 m high along the F_1 fault zone observed at Loc.3. For location see Fig. 10b. (e) and (f) are trench section and sketch showing liquefaction of sand–soil and triangular wedge of debris occurring along the F_1 fault zone. The location of trench site is near Loc.2 on Fig. 9a. Note that the charcoal yields a ^{14}C age of 891 ± 51 yr BP.

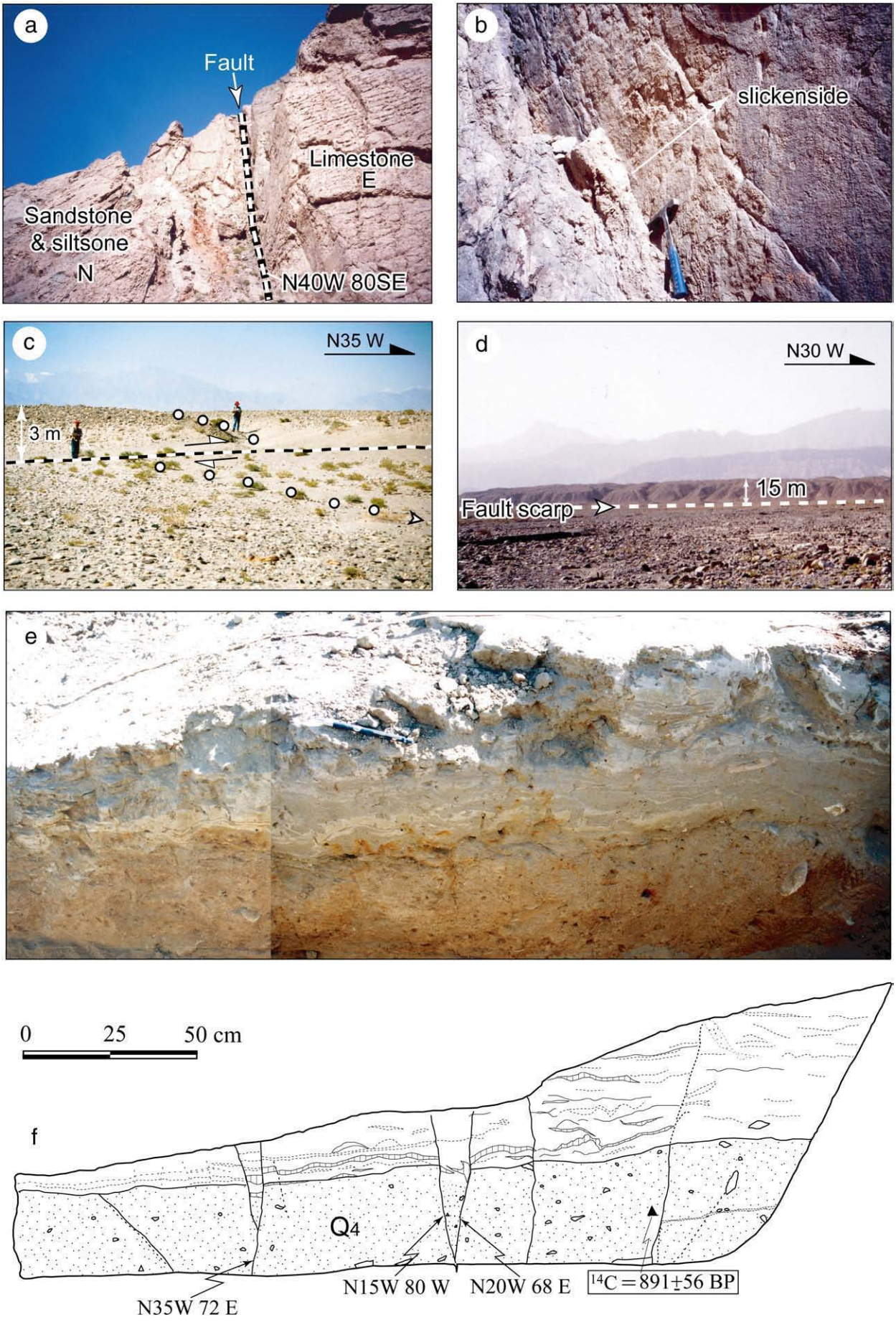
a
Fault
Limestone
E
Sandstone
& siltsone
N
N40W 80SE
b
slickenside
c
N35 W
3 m
d
N30 W
15 m
Fault scarp
e
0 25 50 cm
f
Q4
N35W 72 E
N15W 80 W
N20W 68 E
14C = 891±56 BP

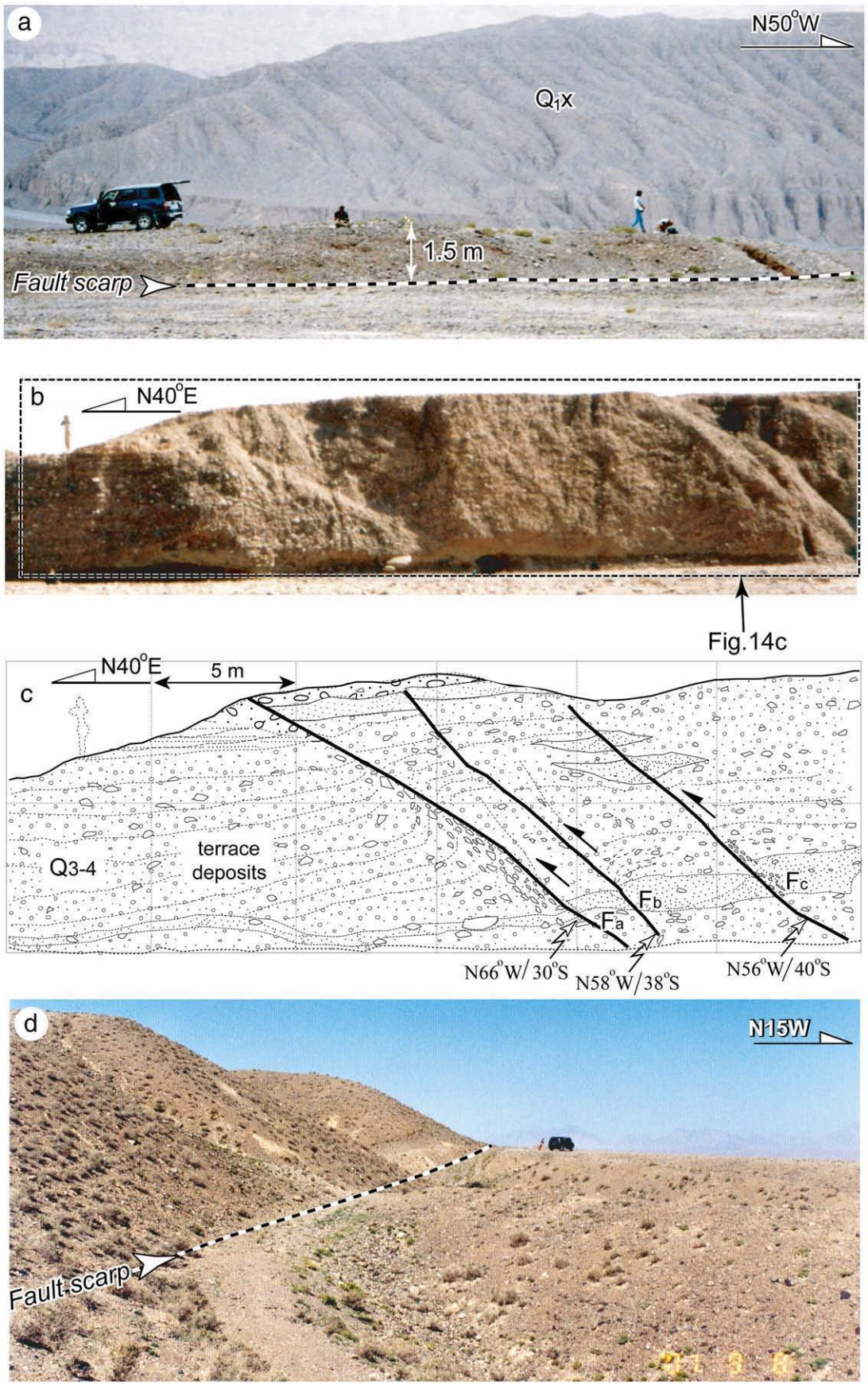

Fig. 14. (a) F_3 fault displaced the late Quaternary terrace deposits. The fault scarp is about 1.5 m high. Observed at the eastern bank of the Kapaka river. For location see Loc.4 on Fig. 11b. (b) Photograph and sketch (c) showing the geomorphic features and occurrence of the co-seismic fault zone related to the 1985 Ms 7.4 Wuqia earthquake. Location is shown as Loc.4 on Fig. 11b. (d) A fault scarp 15–20 m high occurred along the F_5 fault. For scale see Toyota jeep. Location is given by Loc.6 on Fig. 11b.

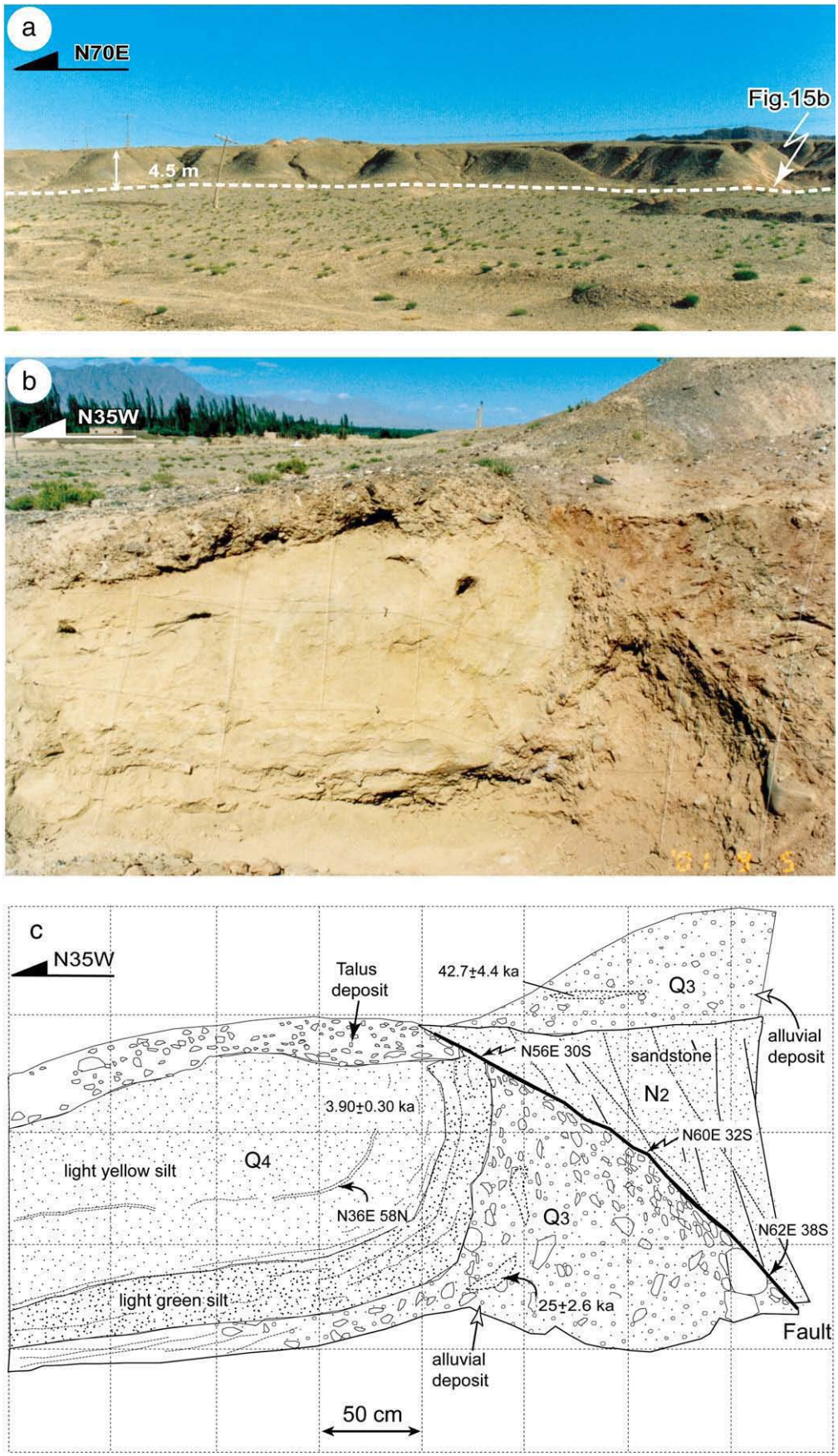

Fig. 15. (a) A photograph displaying the typical fault scarp with a 4–5 m high along the F_4 fault zone to the north of Atushi. (b) Outcrop of active fault revealed by the trench at Loc.8. (c). Sketch showing the occurrence of the active fault. Note that the active fault displaced the Q_3 and Q_4 alluvial deposits (TL dating age after Shen et al. 2001 and Yang et al., 2009). For location of Loc.8 see Fig. 12b.

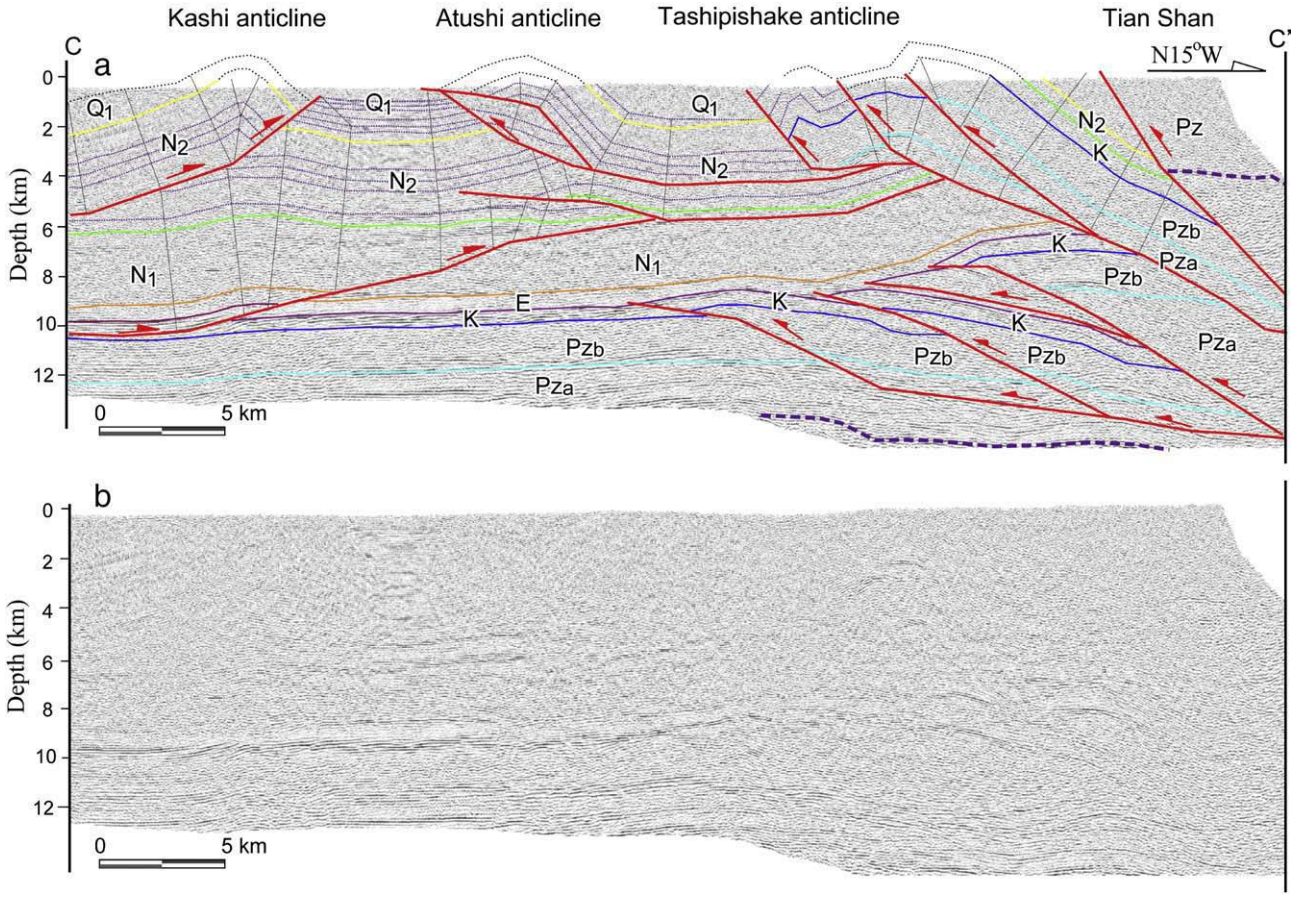

Fig. 16. Structural interpretation and seismic profile across the south Tian Shan and Kashi anticline (modified after Miao et al., 2007).

The F_4 fault is an active thrust fault, which occurs on the north limb of the Atushi–Tanglanghe anticline and displaces the Tertiary to late Quaternary strata (Figs. 11b and 12b). A northward facing fault scarp trends N60°E with 4.5–5 m high at Loc.6 (Fig. 15a). The latest seismic activity here was revealed by trenching (Fig. 15b). As shown on Fig. 15c, late Quaternary deposits with TL and OSL dating age of 3.90 ± 0.30 ka and 25 ± 2.6 ka (Shen et al., 2001; Yang et al., 2009) were displaced by a south-dipping thrust facet that had a vertical displacement of about 1.5 m. The 4.5–5 m high fault scarps were probably produced by three or four large earthquake events. The geologic section shows that this fault is a back thrust on a north-dipping blind thrust beneath the Atushi anticline (Fig. 1b).

The F_5 fault displaces Q_2 deposits in the western segment (Fig. 11b). A north-facing fault scarp of 15 to 20 m high was observed in the field (Fig. 14d). Eastward this fault displaces Tertiary to Lower Pleistocene strata and klippe structures present about 15 km north of Atushi (Fig. 12b). The klippe of rootless lower Pleistocene conglomerate overthrusting on the Miocene strata was observed. Large-scale collapse and gaping faults occur in the Xiyu conglomerate along the F_5 fault (Fig. 12b). Molnar and Deng (1984) inferred that the 1902 Atushi earthquake occurred along this fault zone and epicenter is likely located on the bending part of the fault (Fig. 12b). However, no surface faulting associated with this event has been reported in the past.

The F_6 fault is a north-dipping thrust, which juxtaposes Devonian limestone against Tertiary over lower Pleistocene conglomerates (Figs. 1a, 11b and 12b). We can also find that middle Pleistocene deposits (Q_2) overlap on the Devonian limestone (Figs. 11b and 12b).

The Aheqi (or southern Tian Shan) fault was considered to be the boundary fault between the southern Tain Shan and Tarim basin (AHF in Fig. 1a). Jia et al. (1998) inferred that the Aheqi fault was a left-lateral strike-slip fault. However, they did not show any evidence for this inference (Allen and Vincent, 1999). Along the eastern part of the Aheqi fault, we observed that this fault displaced the late Quaternary alluvial fan deposits and systematic left-lateral offset of stream channels (5 to 15 m) are developed along the fault zone. These observations indicate that the Aheqi fault is an active thrusting fault with some left-lateral component.

5. Discussion

5.1. Slip partitioning in the front of northeastern Pamir

Our results show that the NW-striking faults have extensive dextral strike-slip component in the front of northeastern Pamir (Figs. 1a, 6, 7, 8, 9 and 13). The focal mechanism solution of the 1985 Ms7.4 Wuqia earthquake showed that it is an oblique thrust fault with a large strike-slip component (Fang et al., 1994). However, the amount of separation of oblique convergence into orthogonal strike-slip and reverse components on the NW-striking faults is poorly constrained. The maximum vertical and horizontal displacements observed along the rupture zone of the 1985 Wuqia earthquake were approximately 0.5–1.5 m and 1.8 m, respectively (Feng et al., 1987). It suggests that the amount of strike-slip displacement is larger than the vertical displacement in the western part of the fault. Our results indicate that strike-slip offsets of the gullies along the F_1 fault zone can be divided into four groups: 4.0–4.9 m, 5.3–6.8 m, 8.9–12.8 m, and 14.3–20.4 m as described above. The offset of 4.0–4.9 m is likely produced by the latest seismic event, and the offsets of 14.3–20.4 m

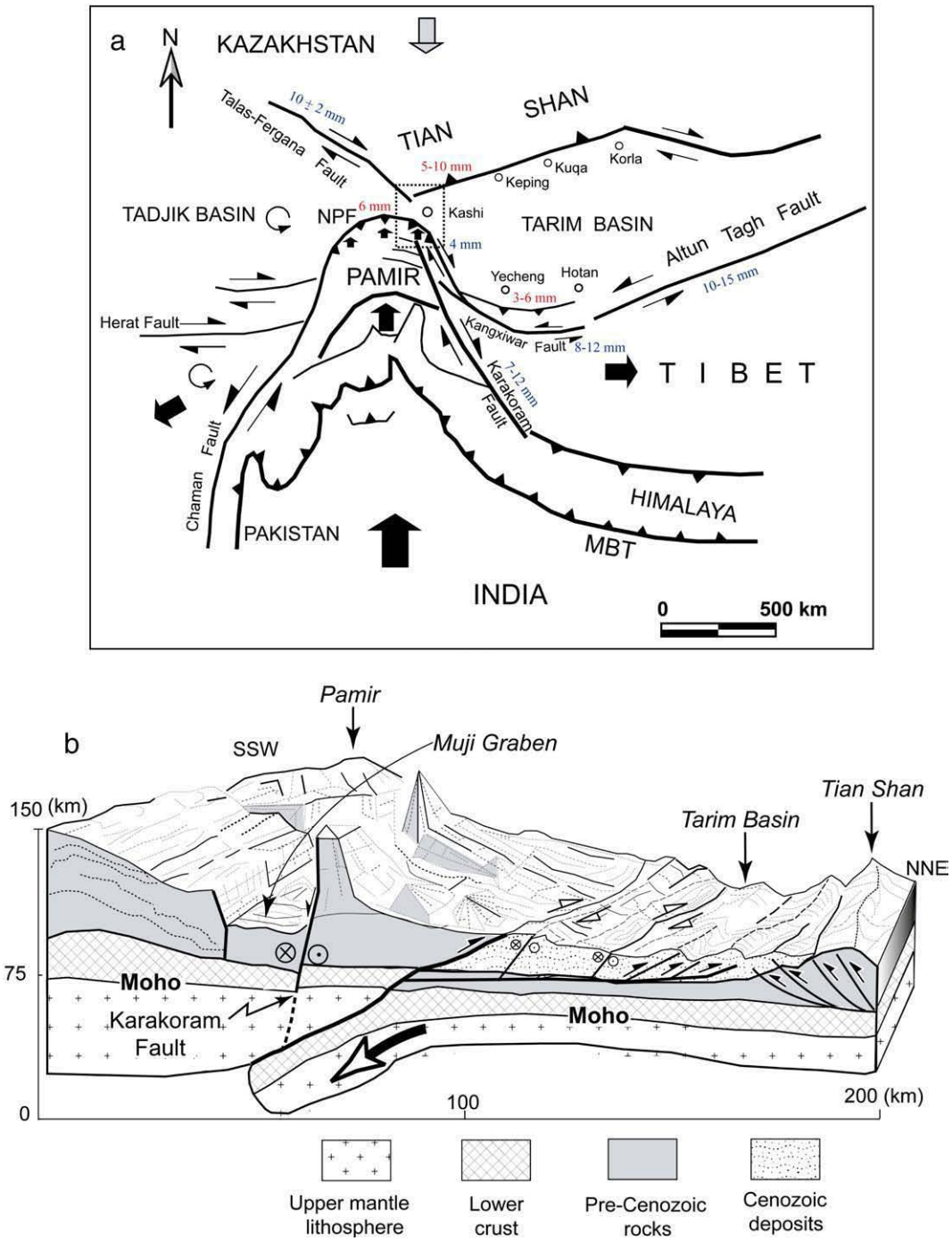

Fig. 17. (a) Major late Cenozoic faults along the Pamir indentor and adjacent area. Northward push of the Pamir and western Kunlun onto the Tarim accompanied crustal thickening and uplift of the Pamir and renewed shortening along the northern margin of Tibet. Reactivated shortening within the Tian Shan resulted in thrusting southward onto the northern margin of the Tarim. Modified from Avouac and Tapponnier (1993) and Searle (1996). Note that red and blue numbers represent shortening and slip rates, respectively. (b) A 3D diagram illustrates the current lithospheric structure, deformation styles and geomorphic features across the northeastern Pamir–Tian Shan convergence zone. Note that southwards deep underthrusting occurs beneath the northern Pamir (deep lithospheric structure modified from Burtman and Molnar, 1993).

are the result of cumulative offsets due to at least three or four seismic events. With an average recurrence interval of 1000 years (Fig. 13f; Feng, 1997) and a strike-slip offset of 4.0–4.9 m, a slip rate of 4.0 ± 1.0 mm/yr is inferred. This estimation is about half of the slip rate of 10 ± 2 mm/yr along the Talus-Fergana fault zone (Burtman et al., 1996, Fig. 17a). But it is similar to the average slip rate of 4 ± 1 mm/yr in the central segment during 11 to 14 ka (Brown et al., 2002) and 6 mm/yr on the southern segment of the Karakoram fault system in the past 11 Ma (Murphy et al., 2000). Arrowsmith and Strecker (1999) reported that the Holocene vertical-slip rate is a minimum 6 mm/yr along the Pamir–Alai region in the apex of northern Pamir arc, where the faults are predominately thrusting. Fault scarps on alluvial terraces with a height 3.5 m and formed in the past 1.4 kyr (Feng et al., 1987), yield an average vertical rate of 2.5 mm/yr in the

front of the northeastern Pamir. This is similar with the average dip-slip rate of 3.5 mm/yr to north of the Atushi (Shen et al., 2001). Thus, the northward oblique thrusting has an important right-lateral component in the front of northeastern Pamir.

5.2. Timing of tectonic deformation

Previous studies (e.g., Meyer et al., 1998; Tapponnier et al., 2001) suggested that the rise of the high Tibetan plateau underwent three main stages since India collided with Eurasia ca 50–55 Ma. The currently emerging plateau, bounded by the Altyn Tagh and Haiyuan Faults in the northeast, is a Plio–Quaternary plateau formed in their third stage (Tapponnier et al., 2001). Some researchers suggested that rapid uplift and unroofing of southern Tian Shan began at ~20 Ma (Sobel and Dumitru, 1997; Yin et al., 1998; Allen et al., 1999). The initiation of tectonic deformation, however, remains poorly known in the Pamir–Tian Shan convergence zone.

Our results indicate that widespread folding of thick Xiyu conglomerates (late Pliocene to early Pleistocene) is present in the study area (e.g. Figs. 1a, 3b, 11b and 12b). Generally, the dip angle of Xiyu conglomerates in those folds varies from 28° to 45°, and locally is near vertical (Fig. 3b and c). Xiyu conglomerate is a conformable with Pliocene (N_2) Atushi Fm. in the study area (Fig. 3b; Zheng et al., 2000). Middle Pleistocene (Q_2) deposits dip from 5° to 15°, and there is a regional unconformity between the Q_1 and Q_2 deposits as shown in Figs. 2 and 4. Faults also juxtapose pre-Cenozoic strata over the Xiyu conglomerates (Figs. 11b and 12b). Growth strata began from the upper part of Pliocene strata (Fig. 4), and the age of boundary between Pliocene and Pleistocene is about 2.6 Ma in the Xinjiang region (BGMXJ, 1993; Chen et al., 1994; Sun et al., 2004). The dextral offset of longest stream channel and Tertiary strata ranges from 8000 to15,000 m along the F_1 fault zone (Figs. 7b and 10b). It also suggests that the faulting began at ~3.5 Ma assuming a long-term slip rate of 4.0 ± 1.0 mm/yr. The tectono-stratigraphic evidences presented above suggest that an extensive deformation began at ~3.5 Ma along the northeastern Pamir–Tian Shan convergence zone.

Several lines of evidence from previous studies also indicate that abrupt deformation occurred during 4.5 Ma to 1 Ma in the northern Tibet and Tian Shan. Considering the Dushanzi and Xiyu conglomerate is the growth strata on the folds, the folding likely began from the early Pliocene (5.3 Ma) to early Pleistocene time (2.6 Ma) in the north and south piedmonts of Chinese Tian Shan (Burchfiel et al., 1999; Fu et al., 2003; Scharer et al., 2004; Sun and Zhang, 2009). In the Kyrgye Tian Shan region, Bullen et al. (2003) indicate an extensive deformation between 4.5 Ma and 1.5 Ma. Similarly, previous studies suggested that extensive deformation began at 4–6 Ma in the Pamir–Alai region of Kyrgyzstan as well as the northwestern front of the Kunlun (e.g. Arrowsmith and Strecker, 1999; Zheng et al., 2000; Wang et al., 2003; Sun and Liu, 2006). All these studies indicate that an extensive Plio–Quaternary deformation was widespread in northwest Tibet and Tian Shan.

Therefore, it is reasonable that the fold-and-thrust system and the related relief in the northeastern Pamir–Tain Shan convergence zone initiated at ~3–5 Ma.

5.3. Regional kinematics and geodynamics of tectonic deformation

The Pamir–Tian Shan convergence zone is a unique example to understand intracontinental ongoing mountain building within the India–Eurasia collision system (Fig. 17a). Unfortunately, much of the region is remote, and thus the regional kinematics has been poorly understood. Although much of its late Cenozoic deformation is explained by the collision and subsequent penetration of India into Eurasia (Molnar and Tapponnier, 1975; Avouac and Tapponnier, 1993; Burtman and Molnar, 1993), and a complete kinematic description of tectonic deformation over the Pamir and Tian Shan has not been available. Existing kinematic models rely on sparse global and regional GPS-derived measurements, which estimate that 40–50 mm/yr of ongoing northward convergence between India and Eurasia is taken up within a zone of more than 2000 km, affecting an area from the Himalayan front to the mountain ranges of Mongolia (Wang et al., 2001; Reigber et al., 2001; Meade, 2007). Geological, seismic, and geodetic evidence suggest that 18 mm/yr of convergence is expressed as current shortening within the Himalayas and Nepal, and much of the ongoing convergence is taken up within the seismically active ranges to the north (Molnar and Deng, 1984; Morgan and Lyon-Caen, 1989; Larson et al., 1999). Recent results from a regional GPS network indicate that up to 40% (13 ± 7 mm/yr) of the total modern convergence between the India–Eurasia plates is accommodated by shortening in the Tian Shan (Abdrakhmatov et al., 1996; Reigber et al., 2001). It is also suggested there that this is a result of a rigid Tarim block rotating clockwise with respect to stable Eurasia about a pole located at 96 °E and 43.5 °N with respect to Siberia ('stable' Eurasia), and herewith transferring deformation from the Himalayas and Tibet to the north. Paleomagnetic data suggest that the ongoing northward penetration of the Pamirs into the Tarim is merging the northern Pamirs with the western Tian Shan together (Burtman and Molnar, 1993; Burtman et al., 1996), and the deformation produced by block rotation is also ongoing between the south Tian Shan and Northern Tarim (Huang et al., 2009). The geologic and geodetic observations agree well in the west Tian Shan, which suggests that the remaining, geodetically calculated shortening of, 5–10 mm/yr should occur in the south Tian Shan and north Tarim (Fig. 17a).

As shown in Fig. 17a, the indentor kinematic model of tectonic deformation can also explain the complex structural patterns around the Pamir, western Tibet during the Plio–Quaternary (Searle, 1996). The western margin of the Pamir indentor is a large-scale sinistral shear zone along the trace of the Chaman fault zone with mainly anticlockwise rotations to the west and northwest (Fig. 17a). Paleomagnetic evidence indicated the anticlockwise rotation of up to 60° in the Tadjik basin (Burtman and Molnar, 1993). East of the Pamir indentor, the Karakoram fault zone has a right-lateral slip rate of 7–12 mm/yr during the late Cenozoic (e.g. Brunel et al., 1994; Searle, 1996). In the northeast front of the Pamir, the oblique convergence caused by the India–Eurasia collision can be accommodated by both S–N directed shortening rate of 6 mm/yr and NW-WNW dextral slip rate of 4 mm/yr (Fig. 17a).

As a result of crustal shortening caused by folding and thrusting as well as block rotation related to strike-slip faulting during late Cenozoic time, the striking present-day relief in the Pamir–Tian Shan convergence zone formed (Fig. 17b).

6. Conclusions

The results from the satellite remote sensing mapping as well as the field geologic and geomorphic observations show that two opposite-vergent fold-and-fault structural belts are present in the northeastern Pamir–Tian Shan convergence zone. The boundary of the two opposite-verging fold-and-fault belts likely distributes between Kashi and Atushi anticlines. In the front of northeastern Pamir, tectonic deformation is characterized by fault-related folding with an extensive dextral strike-slip partitioning. In contrast, the geometry and pattern of the fold-and-thrust belt in the southwest Tian Shan suggest that the fold-and-fault system results from convergence between the Tarim Basin and the Tian Shan. These structural patterns suggest that oblique convergence caused by the India–Eurasia collision can be partitioned into S–N shortening and NW-WNW right-lateral faulting in the study area.

Tectono-stratigraphic evidence suggests that the fold-and-thrust system and the related relief in the northeastern Pamir–Tain Shan convergence zone most likely occurred since ca.3–5 Ma.

Furthermore, our results constrained that the northward oblique thrusting is accommodated by a dextral slip rate of 4.0 ± 1.0 mm/yr in the front of the northeastern Pamir during late Cenozoic time. Extensive current seismic activities occurred within this convergence zone suggesting the ongoing deformation.

In general, the ongoing intracontinental mountain building in the Pamir–Tian Shan convergence zone should be attributed to crustal shortening caused by folding and thrusting as well as block rotation related to strike-slip faulting.

Acknowledgements

B.C. Burchfiel and M.B. Allen provided constructive comments that helped to strengthen an early version of this manuscript. This study was greatly improved by the detailed reviews of two anonymous reviewers. Thanks also to K.I. Kano, A.M. Lin and T. Maruyama for fieldwork. ASTER remote sensing data were provided by the Earth Remote Sensing Data Analysis Center (ERSDAC), Japan. This research was supported by the NSFC project (40721003) and Project of the Knowledge Innovation from Chinese Academy of Sciences (KZCX2-YW-12).

References

Abdrakhmatov, K.Ye., Alddazhanov, S.A., Hager, B.H., Hamburger, M.W., Herring, T.A., Kalabaev, K.B., Makarov, V.I., Molnar, P., Panasyuk, S.V., Prilepin, M.T., Reilinger, R.E., Sadybakasov, I.S., Souter, B.J., Trapezinkov, Yu.A., Tsurkov, V.Y., Zubovich, A.V., 1996. Relatively recent construction of the Tien Shan inferred from GPS measurements of present-day crustal deformation rates. Nature 384, 450–453.

Allen, M.B., Vincent, S.J., 1999. Structural features of the northern Tarim basin: implications for regional tectonics and petroleum traps: discussion. AAPG Bulletin 83, 1279–1283.

Allen, M.B., Vincent, S.J., Wheeler, P.J., 1999. Late Cenozoic tectonics of the Kepingtage thrust zone: interactions of the Tien Shan and Tarim Basin, northwest China. Tectonics 18, 639–654.

Arrowsmith, J.R., Strecker, M.R., 1999. Seismotectonic range-front segmentation and mountain-belt growth in the Pamir–Alai region, Kyrgyzstan (India–Eurasia collision zone). Geological Society of American Bulletin 111, 1665–1683.

Avouac, J.P., Tapponnier, P., 1993. Kinematic model of active deformation in central Asia. Geophysical Research Letters 20, 895–898.

Brown, E.T., Bourles, D.L., Burchfiel, B.C., Deng, Q., Li, J., Molnar, P., Raisbeck, G.M., Yiou, F., 1998. Estimation of slip rates in the southern Tien Shan using cosmic ray exposure dates of abandoned alluvial fans. Geological Society of American Bulletin 110, 377–386.

Brown, E.T., Bendick, R., Bourles, D.L., Gaur, V., Molnar, P., Raisbeck, G.M., Yiou, F., 2002. Slip rates of the Karakorum fault, Ladakh, India, determined using cosmic ray exposure dating of debris flows and moraines. Journal of Geophysical Research 107, 2192–2204.

Brunel, M., Arnaud, N., Tapponnier, P., Pan, Y., Wang, Y., 1994. Kongur Shan normal fault: type example of mountain building assisted by extensional (Karakoram fault, eastern Pamir). Geology 22, 707–710.

Bullen, M.E., Burbank, D.W., Garver, J.I., 2003. Building the northern Tien Shan: integrated thermal, structural, and topographic constraints. The Journal of Geology 111, 149–165.

Burchfiel, B.C., Brown, E.T., Deng, Q.D., Feng, X., Li, J., Molnar, P., Shi, J., Wu, Z., You, H., 1999. Crustal shortening on the margins of the Tien Shan, Xinjiang, China. International Geology Reviews 41, 665–700.

Bureau of Geology and Mineral Resources of Xinjiang Uygur Autonomous Region (BGMXJ), 1993. Regional Geology of Xinjiang Uygur Automomous Region. Geological Publishing House, Beijing, p. 841.

Burtman, V.S., Molnar, P., 1993. Geological and geophysical evidence for deep subduction of continental crust beneath the Pamir. Geological Society of America Special Paper 281, 1–76.

Burtman, V.S., Skobelev, S.F., Molnar, P., 1996. Late Cenozoic slip on the Talas-Ferghana fault, the Tien Shan, Central Asia. Geological Society of America Bulletin 108, 1004–1021.

Chen, H., Lin, X.L., Guan, K.N., Xu, J.M., 1994. Early Pleistocene deposits and it lower boundary (Q/N) in Tian Shan, Xinjiang. Quaternary Science 1, 38–47.

Chen, J., Burbank, D.W., Scharer, K.M., Sobel, E., Yin, J., Rubin, C., Zhao, R., 2002. Magnetochronology of the upper Cenozoic strata in the southwestern Chinese Tian Shan: rates of Pleistocene folding and thrusting. Earth and Planetary Science Letters 195, 113–130.

Dong, D., Xiao, A., 1998. Petroleum Geology and Hydrocarbon Resources in the Southwest Depression of Tarim Basin. Petroleum Industrial Press, Beijing, p. 206.

Fang, G.W., Ni, J.F., Wallace, T.C., 1994. Active tectonics of the Pamirs and Karakorum. Journal of Geophysical Research 99, 7131–7160.

Feng, X., 1997. The Paleoearthquakes in Xinjiang Region, China. Xinjiang Science, Technology and Hygiene Press, Urumqi, p. 260.

Feng, X., Luan, C., Li, J., Kou, D., Yang, Z., 1987. Study on paleoearthquakes in the Kazkearte fault. Inland Earthquakes 1, 231–239.

Fu, B., Lin, A., Kano, K., Maruyama, T., Guo, J., 2003. Quaternary folding of the eastern Tian Shan, northwest China. Tectonophysics 369, 79–101.

Fu, B., Lin, A., Kano, K., Maruyama, T., Guo, J., 2004. Application of stereoscopic satellite images for studying the Quaternary tectonics in the arid regions. International Journal of Remote Sensing 25, 537–547.

Huang, B.C., Piper, J.D.A., Zhu, R.X., 2009. Paleomagnetic constraints on neotectonic deformation in the Kashi depression of the western Tarim Basin, NW China. International Journal of Earth Sciences 98, 1469–1488. doi:10.1007/s00531-008-0401-5.

Jia, D., Lu, H., Cai, D., Wu, S., Shi, Y., Chen, C., 1998. Structural features of the northern Tarim basin: implications for regional tectonics and petroleum traps. American Association of Petroleum Geologists Bulletin 82, 147–159.

Larson, K.M., Burgmann, R., Bilham, R., Freymueller, J., 1999. Kinematics of the India–Eurasia collision zone from GPS measurements. Journal of Geophysical Research 104, 1077–1093.

Lin, A., Fu, B., Kano, K., Maruyama, T., Guo, J., 2002. Late Quaternary right-lateral displacement along the active faults in the Yanqi basin, southeastern Tian Shan, northwest China. Tectonophysics 354, 157–178.

Meade, B.J., 2007. Present-day kinematics at the India–Asia collision zone. Geology 35, 81–84.

Meyer, B., Tapponnier, P., Bourjot, L., Metiver, F., Gaudemer, Y., Peltzer, G., Guo, S., Chen, Z., 1998. Crustal thickening in Gansu-Qinghai, lithospheric mantle subduction, and oblique, strike-slip controlled growth of the Tibet plateau. Geophysical Journal International 135, 1–47.

Miao, J.J., Jia, C.Z., Hou, X.H., Wang, Z.M., Zou, C.N., Tang, L.J., Song, Y.B., 2007. Structural analysis on Cenozoic fold-and thrust belts in Kashi area, western Tarim basin. Chinese Journal of Geology 42, 740–752 (in Chinese with English abstract).

Molnar, P., Deng, Q., 1984. Faulting associated with large earthquakes and the average rate of deformation in central and eastern Asia. Journal of Geophysical Research 89, 6203–6227.

Molnar, P., Tapponnier, P., 1975. Cenozoic tectonics of Asia: effects of continental collision. Science 189, 419–426.

Morgan, P., Lyon-Caen, H., 1989. Fault plane solutions of earthquakes and active tectonics of the Tibetan Plateau and its margins. Geophysical Journal International 99, 123–153.

Murphy, M.A., Yin, A., Kapp, P., Harrison, T.M., Ding, L., Guo, J., 2000. Southward propagation of the Karakoram fault system, southwest Tibet: timing and magnitude of slip. Geology 28, 451–454.

Reigber, Ch., Michel, G.W., Galas, R., Angermann, D., Klotz, J., Chen, J.Y., Papschev, A., Arslanov, R., Tzurkov, V.E., Ishanov, M.C., 2001. New space geodetic constraints on the distribution of deformation in Central Asia. Earth Planet Science Letters 191, 157–165.

Scharer, K.M., Burbank, D.W., Chen, J., Weldon, R.J., Rubin, C., Zhao, R., Shen, J., 2004. Detachment folding in the southwestern Tian Shan–Tarim foreland, China: shortening estimates and rates. Journal of Structural Geology 26, 2119–2137.

Scharer, K.M., Burbank, D.W., Chen, J., Weldon, R.J., 2006. Kinematic models of fluvial terraces over active detachment folds: constraints on the growth mechanism of the Kashi-Atushi fold system, Chinese Tian Shan. Geological Society of America Bulletin 118, 1006–1021.

Searle, M.P., 1996. Geological evidence against large-scale pre-Holocene offsets along Korakoram fault: implications for the limited extrusion of the Tibetan Plateau. Tectonics 15, 171–186.

Shen, Z.K., Zhao, C., Yin, A., Li, Y., Jackson, D.D., Fang, P., Dong, D., 2000. Contemporary crustal deformation in east Asia constrained by GPS measurements. Journal of Geophysical Research 105, 5721–5734.

Shen, J., Zhao, R., Li, J., Burbank, D., Share, K., 2001. Measurements of terrace deformation and crustal shortening rate in the northwest margin of Tarim Basin. Chinese Science Bulletin 46, 334–338.

Sobel, E.R., 1999. Basin analysis of the Jurassic–Lower Cretaceous southwest Tarim Basin, northwest China. Geological Society of America Bulletin 111, 709–724.

Sobel, E.R., Dumitru, T.A., 1997. Thrusting and exhumation around the margins of the western Tarim basin during the India–Asia collision. Journal of Geophysical Research 102, 5043–5063.

Sun, J.M., Liu, T.S., 2006. The age of the Taklimakan desert. Science 312, 1621.

Sun, J.M., Zhang, Z.Q., 2009. Syntectonic growth strata and implications for late Cenozoic tectonic uplift in the northern Tian Shan, China. Tectonophysics 463, 60–68.

Sun, J.M., Zhu, R.X., Bowler, J., 2004. Timing of the Tianshan Mountains uplift constrained by magnetostratigraphic analysis of molasse deposits. Earth and Planetary Science Letters 219 (3–4), 239–253.

Tapponnier, P., Xu, Z., Roger, F., Meyer, B., Arnaud, N., Wittlinger, G., Yang, J., 2001. Oblique stepwise rise and growth of the Tibet Plateau. Science 294, 1671–1677.

Tian, Q., Ding, G., Hao, P., 2006. Seismotectonic study on west part of the interaction zone between southern Tian Shan and northern Pamir. Seismology and Geology 28, 213–223 (in Chinese with English abstract).

Wang, Q.M., Nishidai, T., Coward, M.P., 1992. The Tarim Basin, NW China: formation and aspects of petroleum geology. Journal of Petroleum Geology 15, 5–34.

Wang, Q., Zhang, P.Z., Freymuller, J.T., Bilham, R., Larson, K.M., Lai, X.A., You, X.Z., Niu, Z.J., Wu, J.C., Li, Y.X., Liu, J.N., Yang, Z.Q., Chen, Q.Z., 2001. Present-day crustal deformation in China constrained by global positioning system measurements. Science 294, 574–577.

Wang, E.C., Wan, J.L., Liu, J.Q., 2003. Late Cenozoic geological evolution of the foreland basin bordering the West Kunlun range in Pulu area: constraints on timing of uplift of northern margin of the Tibetan Plateau. Journal of Geophysical Research 108, B82041. doi:10.1029/2002JB001877.

Xinjiang Uygur Autonomous Region Regional Stratigraphic Correlation Group (XJUARRSCG), 1981. Stratigraphic Table of the Northwestern Region: Volume

for Xinjiang Uygur Autonomous Region. Geological Publishing House, Beijing. 496pp.
Yang, X.P., Chen, L.C., Li, A., Du, L., Deng, Q.D., 2009. The uplift of Artux anticline by stages in the Late Quaternary, southwest Tian Shan. Earth Science Frontiers 16, 160–170 (in Chinese with English abstract).
Yin, A., Nie, S., Craig, P., Harrison, T.M., Ryerson, F.J., Qian, X., Yang, G., 1998. Late Cenozoic tectonic evolution of the southern Chinese Tian Shan. Tectonics 17, 1–27.
Zheng, H., Powell, C., An, Z., Zhou, J., Dong, G., 2000. Pliocene uplift of the northern Tibetan Plateau. Geology 28, 715–718.